

# Co(II) Amide, Pyrrolate and Aminopyridinate Complexes: Assessment of their Manifold Structural Chemistry and Thermal Properties

David Zanders,<sup>1,2</sup> Nils Boysen,<sup>1†</sup> Michael A. Land,<sup>2†</sup> Jorit Obenlünenschloß,<sup>1</sup> Jason D. Masuda,<sup>3</sup> Bert Mallick,<sup>4</sup> Seán Barry<sup>2</sup> and Anjana Devi<sup>1\*</sup>

<sup>1</sup>Inorganic Materials Chemistry, Ruhr University Bochum, Universitätsstr. 150, Bochum, 44801 Germany

<sup>2</sup>Department of Chemistry, Carleton University, 1125 Colonel By Drive, Ottawa, Ontario, K1S 5B6 Canada

<sup>3</sup>Department of Chemistry, Saint Mary's University, 923 Robie Street, Halifax, Nova Scotia, B3H 3C3 Canada

<sup>4</sup>Chair of Inorganic Chemistry II, Faculty of Chemistry and Biochemistry, Ruhr-University Bochum, Universitätsstraße 150, Bochum, 44801 Germany

**KEYWORDS** Cobalt, Amides, Transition Metal Complexes, Deposition Precursor, Thermal Analysis

\*Corresponding author: [anjana.devi@rub.de](mailto:anjana.devi@rub.de)

## Abstract:

A series of cobalt(II) (silyl)amides, pyrrolates and aminopyridinates were synthesized. Inspired by the well-known dimeric bis(trimethylsilylamido)cobalt(II) complex ([Co(TMSA)<sub>2</sub>]<sub>2</sub>), facile salt metathesis employing the ligand 2,2,5,5-tetramethyl-1,2,5-azadisilolidinyl (TMADS) yielded its congener bis(2,2,5,5-tetramethyl-1,2,5-azadisilolidinyl)cobalt(II), [Co(TMADS)<sub>2</sub>]<sub>2</sub> exhibiting internally bridged silylamide ligands. Novel, heteroleptic Lewis adducts of the former with unusual three- to four-fold coordination geometry around the metal center were obtained upon reaction with N,N'-di-*tert*-butylethane-1,2-diimine (DAD), N,N-dimethylpyridine-2-amine (DMAPY), and N-*tert*-butyl-1-(pyridine-2-yl)methanimine (IMPY). A similar approach allowed the isolation of the salt [Co(TMADS)<sub>3</sub>Li(DAD)<sub>2</sub>] which renders a rare example of an ion separated Co(II) complex with silylamide ligation and Li<sup>+</sup> counter cation. Straightforward transpyrrolylation utilizing [Co(TMSA)<sub>2</sub>]<sub>2</sub> was established as alternative protocol for the synthesis of bis[N,N'-2-(dimethylaminomethyl)pyrrolyl]cobalt(II), Co(AMPR)<sub>2</sub>, and its structural relative bis(N-2-(*tert*-butyliminomethyl)pyrrolyl)cobalt(II), Co(IMPR)<sub>2</sub>. Treatment of CoCl<sub>2</sub> with two equivalents of lithiated N,N-dimethyl(N'-*tert*-butyl)ethane-1-amino-2-amide (TBUEDMA) and N,N-dimethyl(N'-trimethylsilyl)ethane-1-amino-2-amide (TMSAEDMA) forwarded the respective Co(II) amido-amines as monomeric complexes. Notably, upon salt metathesis reaction of CoCl<sub>2</sub> with two equivalents of lithium 4-

methyl-N-(trimethylsilyl)pyridine-2-amide (TMSMAPY), the first binuclear, homoleptic Co(II) aminopyridinate complex was obtained bearing a strongly distorted trigonal bipyramidal coordination environment ( $\tau_5 = 0.533$ ) for one central Co(II) ion and a weakly distorted tetrahedral coordination geometry ( $\tau_4 = 0.845$ ) for the other. All new compounds were characterized by elemental analyses, IR spectroscopy, and electron ionization mass spectrometry, and their magnetic moments were determined using Evans' method. Additionally, their solid-state structures were determined by single-crystal X-ray crystallography. Finally, the volatility and thermal stability of the compounds were assessed using a combination of thermogravimetric analysis and complementary bulk sublimation experiments.

## Introduction

Ever since Alfred Werner coined the term coordination complex in 1893,<sup>[1]</sup> and was able to exemplify his far-reaching theory using the example of hexol in 1911,<sup>[2]</sup> the coordination chemistry of the later transition metal cobalt (Co) expanded vastly and has been subject of extensive research. Among the many compound classes known to date, there are Co(II) (silyl)amides, pyrrolates and aminopyridinates. With our long-term research focusing on the synthesis of inorganic complexes and their evaluation as precursors for the application in chemical gas phase deposition processes such as metal organic chemical vapor deposition (MOCVD) and atomic layer deposition (ALD),<sup>[3,4]</sup> and our recent interest in the chemistry of the later transition metal Co,<sup>[5]</sup> we identified prior mentioned classes as promising model systems for our studies. Even though operational modes and conditions of MOCVD and ALD processes differ, their complementary and precise applicability for the deposition of a broad range of thin film materials have made them industrially indispensable in fields like microelectronics, optoelectronics and photovoltaics.<sup>[6]</sup> Choosing the right precursor, namely a compound that is volatilized during the process to serve as chemical source for the target material, for a specific application is of crucial importance hereby: The precursor needs to meet demanding requirements such as high thermal stability, sufficient volatility, high but controllable reactivity and lastly non-etching behavior.<sup>[3,4,7]</sup> Reviewing the list of commonly used Co precursors, it becomes apparent that all-nitrogen or predominantly nitrogen coordinated compounds are widely unexplored in terms of their general suitability as precursors and in terms of actual CVD/ALD process development. This is surprising as the two all-nitrogen coordinated precursors Co(II) bis-(di-*tert*-butyl-acetamidinate),<sup>[8]</sup> and Co(II) bis-(di-*tert*-butyl-diazadienyl) (Co(DAD)<sub>2</sub>)<sup>[9]</sup> have led to significant advancements in ALD and material science. While the likely best known Co(II) silylamide [Co(N(SiMe<sub>3</sub>)<sub>2</sub>)<sub>2</sub>]<sub>2</sub> in the following referred to as [Co(TMSA)<sub>2</sub>]<sub>2</sub> has not found application in this field yet, the recent

usage of its Lewis base coordinated congener  $[\text{Co}(\text{TMSA})_2(\text{THF})]$  in ALD<sup>[10]</sup> raises the question if all-nitrogen Lewis adducts of the type  $[\text{Co}(\text{TMSA})_2\text{L}]$  could be viable precursor candidates. In this regard, it is noteworthy, that a number of Co(II) silylamides and Lewis adducts adapted from them have already been studied in recent years in terms of their structural, electronic and magnetic properties.<sup>[11–17]</sup> Beginning with  $[\text{Co}(\text{TMSA})_2]_2$ , Power and coworkers hereby focused on the synthesis and bonding characterization of low-coordinate Co(II) silylamides of the type  $[\text{Co}(\text{TMSA})_2\text{L}]$ ,<sup>[11]</sup> and  $[\text{Co}(\text{N}(\text{SiMe}_3)\text{Dipp})\text{L}]$ ,<sup>[15]</sup> with Dipp being 2,6-diisopropylphenyl and L being a series of Lewis bases ranging from THF and pyridine to several phosphines derivatives. Complementing these efforts, Rabu and coworkers,<sup>[16]</sup> as well as Layfield and coworkers,<sup>[12]</sup> employed carbenes as Lewis bases and brought three-coordinate complexes of the type  $[\text{Co}(\text{TMSA})_2(\text{NHC})]$  into focus. While Layfield studied the rearrangement of the coordinating carbene, Rabu demonstrated well controllable transamination reactions of  $[\text{Co}(\text{TMSA})_2(\text{NHC})]$  type complexes in interplay with the sterically demanding primary amine  $(\text{Dipp})\text{NH}_2$ . Typically, (silyl)amide ligands with considerable molecular weight and steric demand were employed to stabilize the Co(II) ion in these reports. Thus it is consequential that an assessment of the thermal properties of these types of compounds was not a main objective until now. This is likewise applicable to Co(II) pyrrolate and aminopyridinate complexes of which a few examples have been reported but never been compared in terms of structure and thermal properties.<sup>[18–22]</sup>

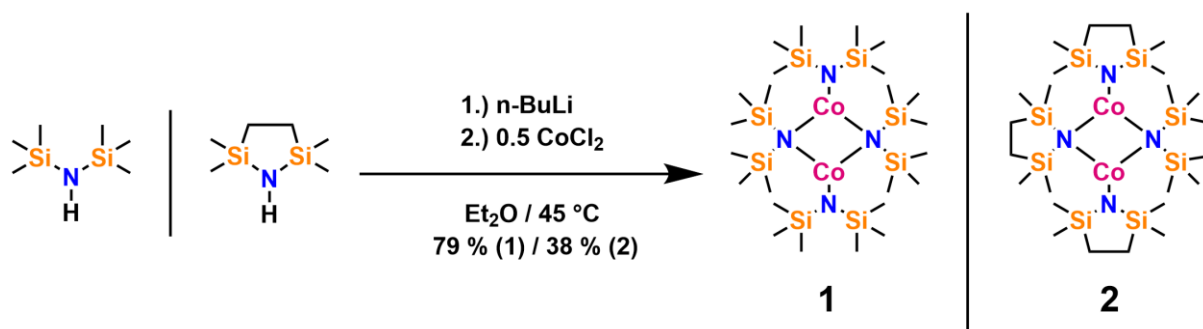
Aiming to broaden the knowledge on selected Co(II) (silyl)amides and some of their Lewis adducts as well as Co(II) pyrrolates and aminopyridinates, this study provides a detailed survey over and comparison of the manifold structural chemistry of in total eleven complexes. First, utilizing the silylamide ligand 2,2,5,5-tetramethyl-1,2,5-azadisilolidinyl, a close structural relative to  $[\text{Co}(\text{TMSA})_2]_2$  is presented. Novel Lewis adducts of the latter with N,N'-di-*tert*-butylethane-1,2-diimine, N,N-dimethylpyridine-2-amine and N-*tert*-butyl-1-(pyridine-2-yl)methaneimine are reported that broaden the number of all-nitrogen low-coordinate Co(II) silylamides. Furthermore, a straightforward and simplified protocol for the synthesis of two related Co(II) pyrrolates by transpyrrolylation of  $[\text{Co}(\text{TMSA})_2]_2$  is described. Hereby, the title compounds, chelated by the N,N'-2-(dimethylaminomethyl)pyrrolyl,<sup>[19]</sup> and N-2-(*tert*-butyliminomethyl)pyrrolyl<sup>[21]</sup> ligand, have been reported prior but not yet been compared in terms of structure and thermal properties. Sharing a chelating nature, the two amido-amino ligands N,N-dimethyl(N'-*tert*-butyl)ethane-1-amino-2-amide and N,N-dimethyl(N'-trimethylsilyl)ethane-1-amino-2-amide are moreover employed to synthesize novel 4-fold coordinated Co(II) amide complexes with distorted tetrahedral geometry. For one of them, the

complete absence of silicon in the ligand sphere renders a rare example and has not been reported for amido-amino ligands of comparable size to the best of our knowledge. Lastly, a rare example of a homoleptic, binuclear Co(II) aminopyridinate complex with a four-fold and a five-fold coordinated Co(II) atom surrounded by four 4-methyl-N-(trimethylsilyl)pyridine-2-amido ligands is described. The synthesis and solid state structures, obtained from single crystal X-ray diffractometry (SC-XRD), of in total eight of the title compounds are reported for the first time. Owing to their respective ligand systems and binding modes, the compounds are divided into four structural categories which allows the identification of multiple similarities and differences that are found to directly affect their thermal stability and volatility in thermogravimetric analysis (TGA) and bulk sublimation experiments. Thus, the present study offers a first structure - thermal property correlation that may be built upon for future, increased exploration of Co(II) (silyl)amides and related compounds as precursors for chemical gas phase deposition.

## Results and Discussion:

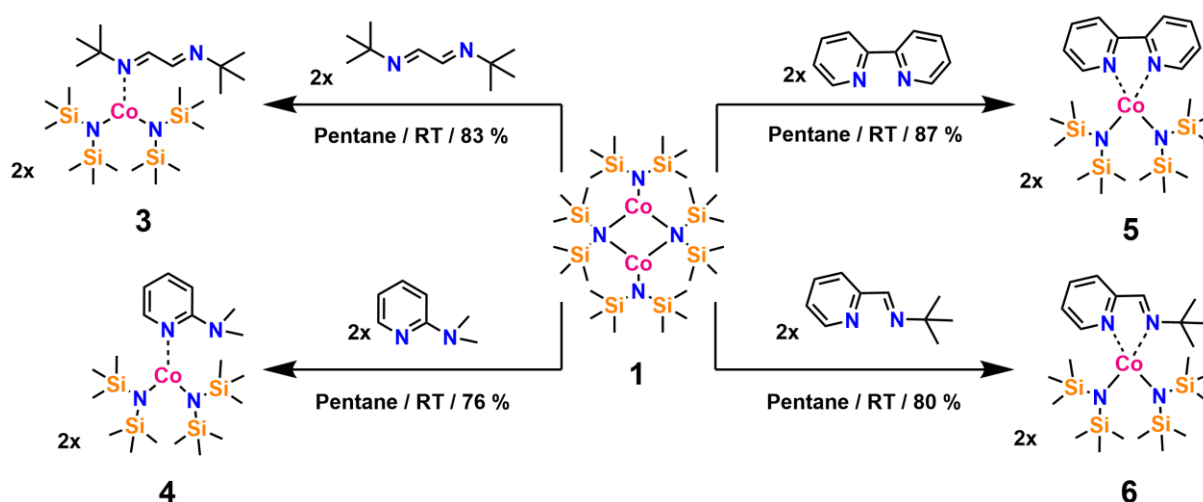
### Synthesis:

To begin our investigation, we first prepared the well-known silylamide  $[\text{Co}(\text{TMSA})_2]_2$  (**1**), following the procedure described by Power and co-workers (**Scheme 1**).<sup>[11]</sup> Additionally, following a similar protocol the 2,2,5,5-tetramethyl-1,2,5-azadisilolidinyl ligated congener  $[\text{Co}(\text{TMADS})_2]_2$  (**2**), was obtained by facile salt metathesis reaction of  $\text{CoCl}_2$  and two equivalents of the respective lithiated silylamide in  $\text{Et}_2\text{O}$ . In both cases, removal of solvent from the dark green solutions was followed by extraction with pentane, and subsequent purification by vacuum distillation. The previously reported silylamide **1** and the hitherto unreported **2** formed dark yellow to green vapors that solidified as dark red to dark brown chunks. We were also able to obtain X-ray quality crystals of **2** which confirmed its solid-state structure (further discussed below). In both cases volatilization occurred concomitant to fractional decomposition of the crude products. The resolidified distillates were then recrystallized from pentane to yield the two title compounds in yields of *ca.* 75% (**1**) and *ca.* 35% (**2**); the lower yield is likely due to increased thermal decomposition during distillation. The effective magnetic moment ( $\mu_{\text{eff}}$  in Bohr magneton  $\mu_{\text{B}}$ ) of the dimeric cobalt compounds **1** and **2** was estimated using the Evans' method (**Table 1**).<sup>[23]</sup> This resulted in values of 5.56  $\mu_{\text{B}}$  and 5.32  $\mu_{\text{B}}$ , respectively. Following the preparation of the dimeric compounds, we speculated that we could break the  $\mu$ -amido bridging bonding motif via addition of ligands that would coordinatively saturate the cobalt center to yield monomeric complexes.



**Scheme 1:** Synthesis of complexes **1** and **2**.

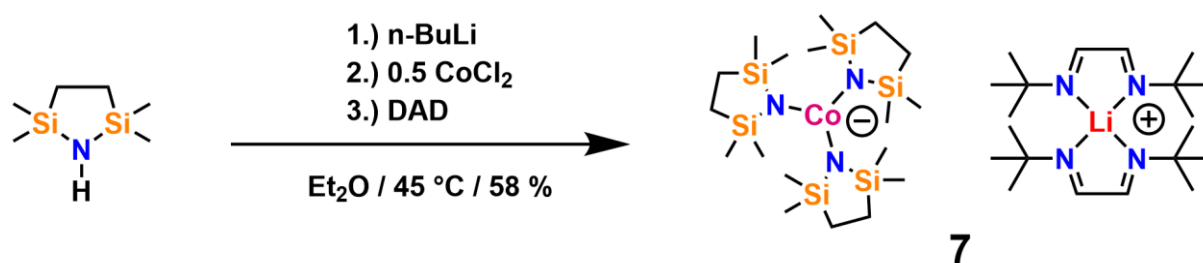
Reaction of dimeric compound **1** at room temperature with a series of nitrogen substituted Lewis bases, namely N,N'-di-*tert*-butylethane-1,2-diimine (DAD), N,N-dimethylpyridine-2-amine (DMAPY), 2,2-bipyridine (BPY), and N-*tert*-butyl-1-(pyridine-2-yl)methanimine (IMPY) yielded the adducts (**3** - **6**) that were crystallized from hydrocarbon solutions as highly colored solids (**Scheme 2**). It should be noted that the synthesis and crystal structure of the BPY adduct **5** has been previously reported,<sup>[17]</sup> yet information on its thermal properties were not provided. Prior to single-crystal X-ray diffraction (SC-XRD) analysis, we hypothesized that [Co(TMSA)<sub>2</sub>(IMPY)] (**6**) might adopt a similar coordination environment around the cobalt center as the BPY adduct **5**, but it was less clear which coordination motives would be present in the bulkier DAD and DMAPY adducts **3** and **4**. In the case of **3** we assumed that it might be favorable for the DAD ligand to adopt a  $\mu$ -bridging bonding mode between two Co(TMSA)<sub>2</sub> fragments similar to what had been observed by König and co-workers for the Lewis base N,N,N',N'-tetra-methyl-ethylene-diamine (TMEDA) in [{Co(TMSA)<sub>2</sub>]<sub>2</sub>(TMEDA)] in case a bidentate chelation should not occur.<sup>[14]</sup> However, elemental analysis revealed only one DAD ligand per cobalt center.



**Scheme 2:** Synthesis of Lewis adduct complexes **3** - **6**.

For **4**, it remained unclear if the N,N-dimethyl-amine in 2-position of the pyridine ligand could contribute to the Co(II) ion coordination or if steric rigidity of the ligand frame would prevent

chelation. Irrespective of these considerations that are addressed in the subsequent section in more detail, **3** - **6** were received in good yields (75 % - 90 %) when prior isolated **1** was converted with the respective Lewis base. The complexes were also accessible from one-pot syntheses using *in-situ* generated **1**. However, this more direct approach resulted in lower yields due to a more difficult workup. Compounds **3** - **6** demonstrated solution effective magnetic moments  $\mu_{\text{eff}}$  of 4.26  $\mu_{\text{B}}$  to 4.75  $\mu_{\text{B}}$  (**Table 1**) which is in a range often observed for  $[\text{Co}(\text{TMSA})_2\text{L}]$  type complexes.<sup>[11,14,16]</sup> Exemplarily, the *in situ* procedure was tested for the reaction of **2** and DAD. Surprisingly, it was not the anticipated  $[\text{Co}(\text{TMADS})_2(\text{DAD})]$  that was isolated, but a salt constituting itself as  $[\text{Co}(\text{TMADS})_3\text{Li}(\text{DAD})_2]$  and herein referred to as **7**. It is a rare example of an ion separated Co(II) cobaltate salt with silylamide ligation and  $\text{Li}^+$  counter cation (**Scheme 3**) and was obtained by crystallization in a yield of 58 %.



**Scheme 3:** Synthesis of the salt  $[\text{Co}(\text{TMADS})_3\text{Li}(\text{DAD})_2]$  **7** following a one pot procedure.

While a few reports on  $[\text{Co}(\text{TMSA})_3]^-$  anions with crown ether ligated  $\text{Li}^+$  or  $\text{Na}^+$  cationic counterparts can be found in the literature,<sup>[13,24]</sup>  $[\text{Co}(\text{TMADS})_3]^-$  ion separated complexes have not been reported yet. On the contrary, the formation of a  $[\text{Li}(\text{DAD})_2]^+$  counter cation has been observed by Gardiner and co-workers in their study on neutral and anionic Al(III) diamine compounds.<sup>[25]</sup>

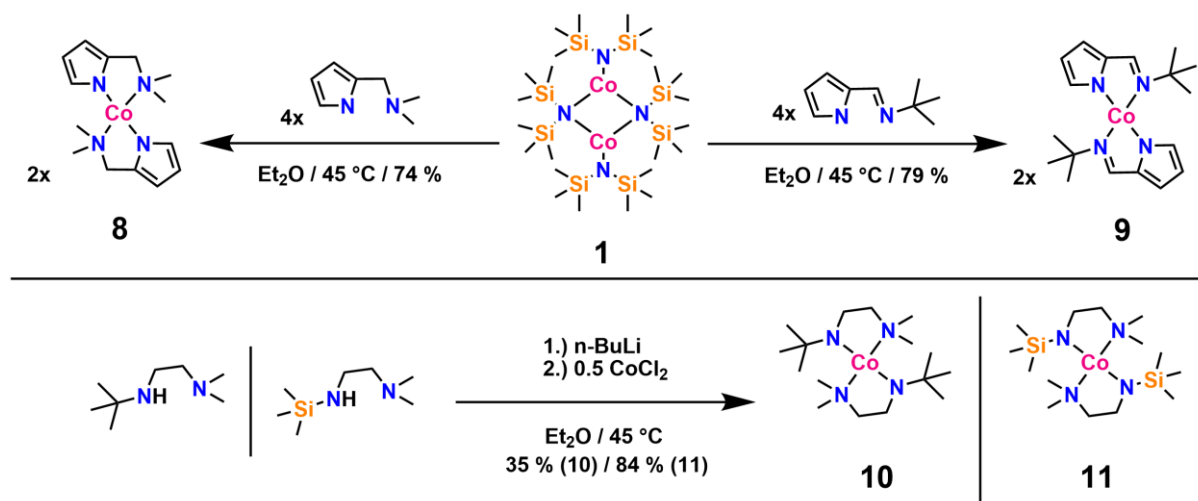
**Table 1:** Solution effective magnetic moments  $\mu_{\text{eff}}$  of cobalt(II) title compounds derived from the Evans method.<sup>[23]</sup>

Compound	$\mu_{\text{eff}}$ ( $\mu_{\text{B}}$ )
$[\text{Co}(\text{TMSA})_2]_2$ <b>1</b>	5.56
$[\text{Co}(\text{TMADS})_2]_2$ <b>2</b>	5.32
$[\text{Co}(\text{TMSA})_2(\text{DAD})]$ <b>3</b>	4.26
$[\text{Co}(\text{TMSA})_2(\text{DMAPY})]$ <b>4</b>	4.75
$[\text{Co}(\text{TMSA})_2(\text{BPY})]$ <b>5</b>	4.49
$[\text{Co}(\text{TMSA})_2(\text{IMPY})]$ <b>6</b>	4.36
$[\text{Co}(\text{TMADS})_3\text{Li}(\text{DAD})_2]$ <b>7</b>	5.01
$\text{Co}(\text{AMPR})_2$ <b>8</b>	4.40
$\text{Co}(\text{IMPR})_2$ <b>9</b>	4.22
$\text{Co}(\text{TBUAEDMA})_2$ <b>10</b>	4.85
$\text{Co}(\text{TMSAEDMA})_2$ <b>11</b>	4.64
$[\text{Co}(\text{TMSMAPY})_2]_2$ <b>12</b>	5.21

It is noteworthy to highlight again, that the same one-pot procedure employing two equivalents of  $\text{Li}(\text{TMSA})$ , one equivalent of  $\text{CoCl}_2$  and even two to threefold excess of DAD only

forwarded compound **3** and that we were not able to isolate cobaltate salt  $[\text{Co}(\text{TMSA})_3\text{Li}(\text{DAD})_2]$ . While it was beyond the scope of this study, we perceive compounds **3** and **7** to be appealing model systems for theoretical studies such as ion pair binding energy calculations that may shed light on their electronic properties which in turn could help to explain the formation of vastly different solid state structures. Determination of the solution magnetic moment *via* Evans' method showed that  $[\text{Co}(\text{TMADS})_3\text{Li}(\text{DAD})_2]$  follows the trend of the previously discussed Co(II) complexes **1** – **6**: With  $\mu_{\text{eff}}$  being  $5.01 \mu_{\text{B}}$ , compound **7** displays a solution effective magnetic moment significantly larger than what is expected for high-spin Co(II) ions according to the spin only equation ( $3.87 \mu_{\text{B}}$ ). Interestingly, Eichhöfer's salt  $[\text{Co}(\text{TMSA})_3\text{Li}(\text{15-crown-5})]^{[13]}$  containing the  $[\text{Co}(\text{TMSA})_3]^-$  anion and crown ether ligated  $\text{Li}^+$  cation exhibited an even higher  $\mu_{\text{eff}}$  value of  $5.25 \mu_{\text{B}}$  at room temperature for solid samples. These high values can generally be ascribed to the emergence of magnetic anisotropy within Co(II) complexes and salts.

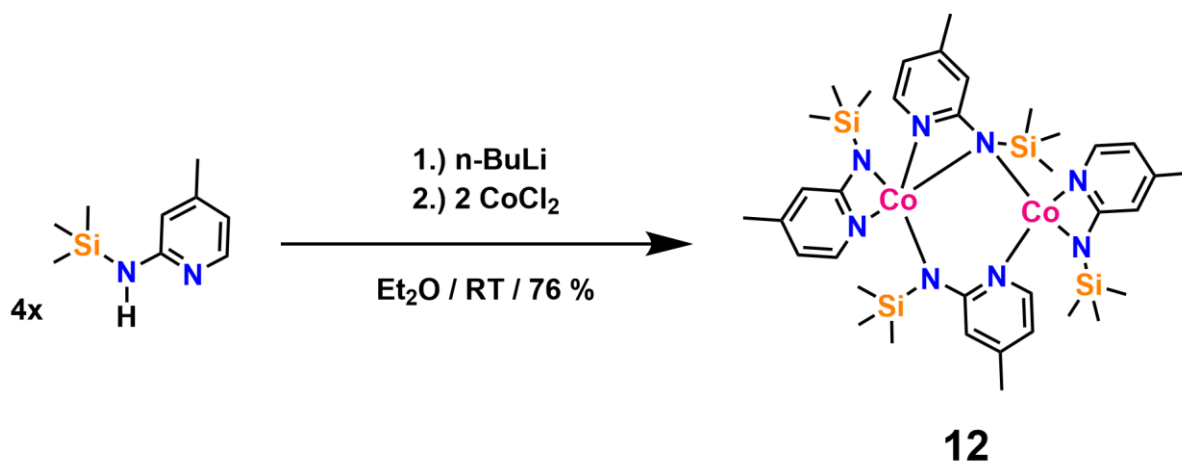
Pyrrolate type ligands such as N,N-dimethyl-1-(pyrrol-2-yl)methanamine (AMPR) and N-*tert*-butyl-1-(pyrrol-2-yl)methanimine (IMPR) have found use for in variety of transition metal complexes.<sup>[26]</sup> For the two Co(II) pyrrolate complexes  $\text{Co}(\text{AMPR})_2$  (**8**) and  $\text{Co}(\text{IMPR})_2$  (**9**) Dreves<sup>[19]</sup> and Holm<sup>[22]</sup> had originally described elaborate and time-consuming multistep synthesis procedures that we found to be avoidable by a direct transpyrrolylation approach employing **1** and the respective protonated pyrrole derivate in  $\text{Et}_2\text{O}$  under mild refluxing conditions for several hours. This preparation method allowed to isolate the crude products nearly quantitatively with subsequent crystallization (**8**) or sublimation (**9**) giving the purified title compounds in yields of ~ 75 % - 80 % as brown-red to red solids (**Scheme 4**).



**Scheme 4:** Synthesis of complexes **8** - **11**.

The solution effective magnetic moments (**Table 1**) were estimated to be  $4.40 \mu_B$  and  $4.22 \mu_B$  respectively which is higher than what is expected based on the spin only approximation for Co(II) high spin complexes ( $3.87 \mu_B$ ) but well within the range often observed experimentally.

In a next step, we aimed to synthesize Co(II) complexes bearing chelating amido-amine ligands and decided to introduce the two closely related ligands N,N-dimethyl(N'-*tert*-butyl)ethane-1,2-diamine (H-TBUAEDMA)<sup>[27]</sup> and N,N-dimethyl(N'-trimethylsilyl)ethane-1,2-diamine (H-TMSAEDMA).<sup>[28]</sup> Employing a standard salt metathesis route, Co(TBUAEDMA)<sub>2</sub> (**10**) and Co(TMSAEDMA)<sub>2</sub> (**11**) were obtained as black and purple solids from 1:2 reaction of CoCl<sub>2</sub> with the respective lithiated amido-amine in refluxing Et<sub>2</sub>O. Subsequent removal of solvent from the intensely colorized solution was followed by extraction of the crude product from pentane, filtration and again solvent removal (**Scheme 4**). Noteworthy, the high solubility of both title compounds in ethers and hydrocarbons was found to impede crude product purification, so vacuum sublimation was attempted instead. Here, despite the strong congruity of the ligand systems, a vast difference between **10** and **11** not in terms of volatility (for both 80 °C at  $1 \times 10^{-1}$  mbar was applied) but regarding thermal stability became apparent for the first time. While the trimethylsilyl side chain substituted amide **11** was repeatedly obtained in good yields of ~ 80 % - 85 %, the yields amounted only to ~ 30 % - 35 % for **9** possessing the *tert*-butyl side chain substituted amides. This can be seen as a further illustration of the superior stabilization capability of  $\beta$ -silylamides in direct comparison to  $\beta$ -carboamides.<sup>[29]</sup> Evans' method forwarded solution magnetic moments of  $4.85 \mu_B$  (**10**) and  $4.64 \mu_B$  (**11**). With the intention to synthesize a monomeric, homoleptic Co(II) aminopyridinate complex, lithiated 4-methyl-N-(trimethylsilyl)pyridine-2-amide (Li-TMSMAPY) was prepared according to a literature reported procedure,<sup>[30]</sup> and reacted with CoCl<sub>2</sub> (2:1 ratio) in boiling Et<sub>2</sub>O for 12 h (**Scheme 5**).



**Scheme 5:** Synthesis of binuclear complex **12**.



After solvent removal, re-dissolution in pentane and filtration, a clear dark green solution was obtained from which SC-XRD quality crystals grew upon storage at -30 °C overnight. A second batch of crystalline material was obtained from the concentrated mother liquor upon cooling (overall yield 75 %). X-ray analysis revealed the dimeric nature of the title compound and displayed rare and deviating coordination environments for the two Co(II) ions. A more detailed description is provided in the subsequent section. Considering the dimeric nature of **12** [Co(TMSMAPY)<sub>2</sub>]<sub>2</sub> in the solid state and hypothesizing **12** to be a dimer in solution as well, the effective magnetic moment was estimated to be 5.21  $\mu_B$ . It is thus similar to the magnetic moments determined for the dimeric **1** and **2** despite the fact that the coordination environment for the Co(II) ions differs notably.

### Structural Analysis:

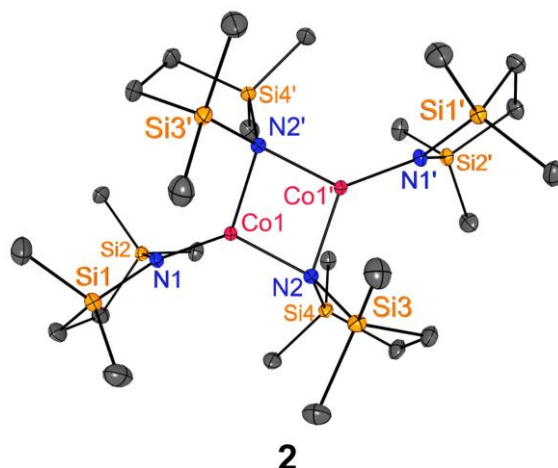
All complexes for which solid state structures are presented were found to either crystallize in monoclinic or orthorhombic space groups as it has exemplarily been observed for several of Lewis adducts of the general type [Co(TMSA)<sub>2</sub>L].<sup>[11,14]</sup> Further information on the crystallographic data and data acquisition parameters are displayed in **Table 2**. For selected compounds, namely **4** and **10 - 12**, additional comments on the disorders found in the measured crystals can be found in the SI (section 4).

**Table 2:** Crystallographic data of all cobalt(II) complexes presented in this study for the first time.

	<b>2</b>	<b>3</b>	<b>4</b>	<b>6</b>	<b>7</b>	<b>8</b>	<b>10</b>	<b>11</b>	<b>12</b>
<i>fw</i> (g mol <sup>-1</sup> )	751.37	547.99	501.89	541.95	877.56	305.28	377.59	345.43	835.14
<i>T</i> (K)	100	100	100	100	100	100	100	100	100
<i>space group</i>	monoclinic P2 <sub>1</sub> /c	monoclinic P2 <sub>1</sub> /n	orthorhombic Pbca	monoclinic P2 <sub>1</sub> /c	monoclinic P 1 2 <sub>1</sub> 1	monoclinic P2 <sub>1</sub>	orthorhombic P2 <sub>1</sub> 2 <sub>1</sub> 2	orthorhombic Pbca	monoclinic P2 <sub>1</sub> /c
<i>a, b, c</i> (Å)	20.9366(17) 10.8818(9) 17.5727(9)	9.6913(4) 16.8156(6) 20.23605(8)	18.7791(4) 14.7461(4) 20.9325(5)	14.1070(2) 12.2007(2) 18.2082(3)	15.3443(1) 15.9200(1) 22.1358(1)	9.0966(3) 14.6418(5) 11.7787(4)	29.1330(7) 16.4473(5) 8.9796(2)	9.7550(2) 15.5832(4) 26.8279(6)	17.6608(3) 11.9329(2) 21.4750(3)
<i>α, β, γ</i> (°)	90.406(3)	102.488(1)	-	97.746(2)	93.530(1)	106.055(4)	-	-	94.541(2)
<i>V</i> (Å <sup>3</sup> )	4003.5(5)	3239.6(2)	5796.6(2)	3105.31(9)	5397.10(5)	1507.62(9)	4302.6(6)	4078.2(2)	4511.5(1)
<i>Z</i>	4	4	8	4	4	4	4	8	4
<i>d<sub>calc</sub></i> (g cm <sup>-3</sup> )	1.247	1.124	1.150	1.159	1.080	1.345	1.166	1.125	1.230
<i>R<sub>i</sub></i> <sup>a</sup>	0.0252	0.0229	0.0543	0.0493	0.0327	0.0379	0.0474	0.0696	0.0317
<i>wR<sub>2</sub></i> <sup>b</sup>	0.0627	0.0622	0.1238	0.1292	0.0860	0.0860	0.1125	0.1802	0.0787
<i>GOF</i> <sup>c</sup>	1.045	1.088	1.040	1.089	1.049	0.983	1.052	1.062	1.035

$$^a R_i = \Sigma(|F_o| - |F_c|)/\Sigma|F_o|, F_o > 2\sigma(F_o), ^b wR_2 = \{\Sigma[w(F_o^2 - F_c^2)^2]/\Sigma[w(F_o^2)^2]\}^{1/2}, ^c GOF = [\Sigma w(F_o^2 - F_c^2)^2/(n_0 - n_p)]^{1/2}.$$

Counterfeiting the prior reported [Co(TMSA)<sub>2</sub>]<sub>2</sub> (**1**), [Co(TMADS)<sub>2</sub>]<sub>2</sub> (**2**), whose solid state structure is illustrated in **Figure 1**, is arranged as a dimer. It exhibits two three-coordinate Co(II) ions that are bridged through two amido ligands while additionally being bonded to a terminal amido ligand each.



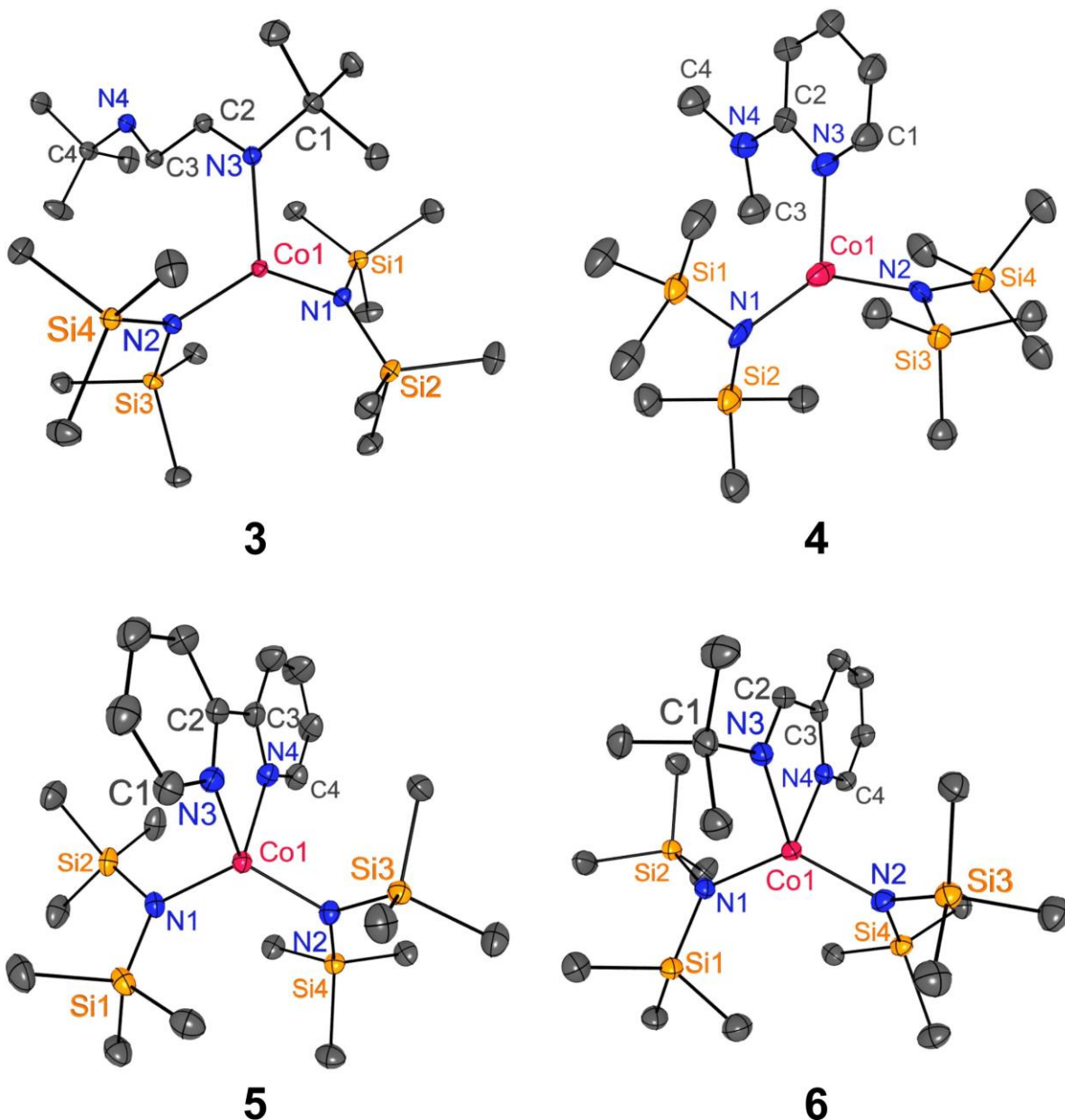
**Figure 1:** Solid state structure of  $[\text{Co}(\text{TMADS})_2]_2$  (**2**) drawn with thermal ellipsoids at 50 % probability level. Hydrogens are omitted for clarity.

With 2.6133(5) Å, the Co $\cdots$ Co interatomic distance between both ions is slightly elongated in comparison to **1** where this distance was found to be 2.5864(5) Å. Yet, the bridging and terminal Co–N binding lengths were slightly shorter with 1.9957(8) Å and 1.8907(7) Å respectively (**Table 3**). Consideration of the Co<sub>2</sub>N<sub>2</sub> core structures revealed a pronounced difference between **1** and **2**: Contrasting the perfectly plain arrangement of the rhomb spanned between Co1, N2, Co1' and N2' in **1**, the nitrogen atoms N2 and N2' in closely related **2** vaulted upwards of the plane that can be defined between Co1 and Co1'. Accordingly, a notable dihedral angle of 10.777(30) ° between the two planes N2–Co1–N2' and N2–Co1'–N2' was created. The distortion of the Co<sub>2</sub>N<sub>2</sub> core structure seen in **2** is likely enforced by the rigidity and strain within the cyclic TMADS amide ligands that does not allow relaxation of the core motif as seen in **1**. While the N–Si bond lengths in both structures are nearly identical and deviate only slightly, the Si–N–Si angles for the bridging as well as the terminal amides are 8 ° smaller in **2** (105.390(39) ° and 107.927(40) °) than in **1** (112.314(45) ° and 118.746(18) °). More importantly, the silyl groups in the ligand backbone are tied together through a CH<sub>2</sub>–CH<sub>2</sub> bridge which does not allow reorientation of the ligand periphery as freely as in **1**. The average Si–C–C–Si distortion angle amounts to 31.59 °. A variety of coordination motives was observed for the solid state structures of the Lewis adduct compounds **3** - **6**: Initially it was postulated that the DAD ligand in **3**, [Co(TMSA)<sub>2</sub>(DAD)], would function as a bidentate Lewis base that would facilitate a four-fold coordination environment around the Co(II) ion. This reasoning was based on the prior demonstrated chelating coordination of DAD in [CoCl<sub>2</sub>(DAD)].<sup>[31]</sup> In opposition to this, the Lewis base was found to bind with only one of the imine nitrogen atoms in a monodentate fashion, while the other imine moiety was averted from the central ion (**Figure 2**).

**Table 3:** Selected Interatomic Distances and Angles of Complexes **1**,<sup>[11]</sup> and **2**.

	<b>1</b> [Co(TMSA) <sub>2</sub> ] <sub>2</sub>	<b>2</b> [Co(TMADS) <sub>2</sub> ] <sub>2</sub>
Bond Lengths / Interatomic Distances (Å)		
Co1–N1	1.9105(11)	1.8907(7)
Co1–N2	2.0602(9)	1.9957(8)
Co1–N2'	2.0602(9)	2.0422(7)
Co1---Co1'	2.5864(5)	2.6133(5)
N1–Si1	1.7367(7)	1.7353(7)
N1–Si2	1.7367(7)	1.7401(8)
N2–Si3	1.7863(12)	1.7711(8)
N2–Si4	1.7834(8)	1.7767(8)
Angles (°)		
N1–Co1–N2	128.761(25)	132.298(34)
N1–Co1–N2'	128.761(25)	129.434(30)
N2–Co1–N2'	102.477(36)	98.210(28)
Co1–N2–Co1'	77.668(28)	80.869(27)
Co1–N2–Co1'–N2'	0.000(36)	10.777(30)
Si1–N1–Si2	118.746(18)	107.927(40)
Si3–N2–Si4	112.314(45)	105.390(39)

Similarly, the dimethylamide moiety of the DMAPY ligand in complex **4**, [Co(TMSA)<sub>2</sub>(DMAPY)], pointed away from the Co(II) ion which was only coordinated by the pyridine nitrogen atom (**Figure 2**). While it likely was the rigidity of the DMAPY ligand paired with localized electron-richness of the pyridine nitrogen that prevented a chelating bonding mode of the Lewis base in **4**, we attributed the three-fold coordination seen in **3** to the considerable special demand of the *tert*-butyl side chains. These may tolerate the coordination of only one imine nitrogen to the Co(II) ion at a time. As it can be seen from **Table 4**, the Co–N bond lengths between the Co(II) ion and the two terminal TMSA ligands in **3** and **4** (~ 1.92 Å and ~1.95 Å respectively) were slightly elongated in comparison to the one found in parent complex (~1.91 Å, **Table 3**). The monodentate imine nitrogen of the Lewis base in **3** exhibited a distance of 2.0892(7) Å to the Co(II) ion, which is only slightly longer than the bridging Co–N bonds found in **1** that complete the trigonal square planar coordination. Contrasting this the Co–N bond length for the pyridine nitrogen in **4** was found to be 2.1416(37) Å and thus noticeably longer. For compound **3**, C–N and C–C bond lengths listed in **Table 4** suggest that there is no delocalization of electron density within the Lewis base. Likewise, no alternation of the Lewis base backbone in **4** was observed. With  $\Sigma^0 = 359.88(6)$  for **3** and  $\Sigma^0 = 359.31(7)$  for **4**, the two Lewis adduct complexes exhibit an expected trigonal planar geometry at their Co(II) ions. Interestingly, the N1–Co1–N3 and N2–Co1–N3 angles which span between the TMSA ligands and the Lewis base, are nearly the same for **3** (115.500(3) ° and 114.561(29) °) while they are considerably different for **4** (129.118(586) ° and 98.406(646) °).



**Figure 2:** Solid state structures of  $[\text{Co}(\text{TMSA})_2(\text{DAD})]$  (**3**),  $[\text{Co}(\text{TMSA})_2(\text{DMAPY})]$  (**4**),  $[\text{Co}(\text{TMSA})_2(\text{BPY})]$  (**5**) and  $[\text{Co}(\text{TMSA})_2(\text{IMPY})]$  (**6**) drawn with thermal ellipsoids at 50 % probability level. Hydrogens are omitted for clarity. The structure of **5** is reproduced from the data provided by Müller and co-workers.<sup>[17]</sup>

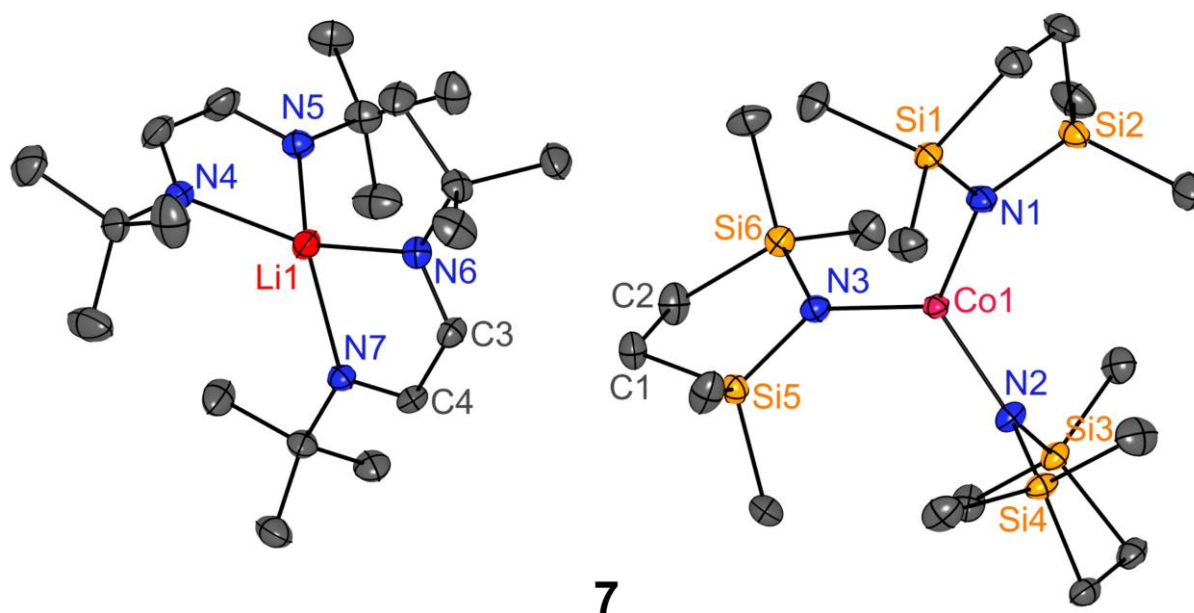
It is a consequence of a preferential tilt of the DMAPY ligand towards one of the TMSA ligands. Somewhat different angles of this kind for  $[\text{Co}(\text{TMSA})_2\text{L}]$  type Lewis adducts have been observed prior.<sup>[11]</sup> Just as its prior reported congener  $[\text{Co}(\text{TMSA})_2(\text{BPY})]$  (**5**),  $[\text{Co}(\text{TMSA})_2(\text{IMPY})]$  (**6**) was found to feature a four-fold, distorted tetrahedral coordination environment around the central ion. For both compounds, the increased spatial demand of the Lewis base was found to elongate the Co–N bond lengths between the Co(II) ion and the TMSA ligands.

**Table 4:** Selected Interatomic Distances and Angles of Complexes **3**, **4**, **5**,<sup>[17]</sup> and **6**. Abbreviations used for the four complexes in this study are given for clarity.

	<b>3</b> [Co(TMSA) <sub>2</sub> (DAD)]	<b>4</b> [Co(TMSA) <sub>2</sub> (DMAPY)]	<b>5</b> [Co(TMSA) <sub>2</sub> (BPY)]	<b>6</b> [Co(TMSA) <sub>2</sub> (IMPY)]
Bond Lengths (Å)				
Co1–N1	1.9160(7)	1.9275(197)	1.9586(26)	1.9727(22)
Co1–N2	1.9219(6)	1.9816(210)	1.9605(26)	1.9829(24)
Co1–N3	2.0892(7)	2.1416(37)	2.1215(26)	2.1425(21)
Co1–N4	–	–	2.0989(27)	2.1248(21)
average N–Si	1.72	1.73	1.71	1.71
N3–C1	1.5157(10)	1.3662(65)	1.3337(43)	1.5006(33)
N3–C2	1.2820(11)	1.3550(99)	1.3495(41)	1.2764(32)
N4–C2	–	1.3526(11)	–	–
N4–C3	1.2725(13)	1.4314(69)	1.3473(43)	1.3493(32)
N4–C4	1.4772(11)	1.4412(73)	1.3368(44)	1.3286(34)
C2–C3	1.4678(11)	–	1.4776(48)	1.4722(36)
Angles (°)				
N1–Co1–N2	129.825(32)	131.786(830)	123.266(108)	128.191(94)
N1–Co1–N3	115.500(3)	129.118(586)	100.865(104)	104.493(86)
N1–Co1–N4	–	–	122.002(107)	113.820(89)
N2–Co1–N3	114.561(29)	98.406(646)	123.667(103)	121.397(87)
N2–Co1–N4	–	–	102.081(106)	98.649(90)
N3–Co1–N4	–	–	77.479(102)	78.446(83)
Lewis base fragment twisted with respect to Co(TMSA) <sub>2</sub> moiety (°)				
	55.16	42.95	71.83	77.01
$\tau_4^{[32]} / \tau_4'^{[33]}$				
	–	–	0.802 / 0.801	0.783 / 0.762

For **5** the Co–N bonds were found to average out at  $\sim 1.96$  Å whereas they adopted mean lengths of  $\sim 1.98$  Å for **6** (Table 4). The distances Co1–N3 and Co1–N4 defined between the central ion and the pyridine nitrogen atoms were 2.1215(26) Å and 2.0989(27) Å and are comparable to the Co(II) - pyridine nitrogen distance in **6** (Co1–N4; 2.1248(21) Å). The distance between the ion and the imine nitrogen amounts to 2.1425(21) thus being only slightly longer. In comparison to **3** however, the bond is notably longer. The distorted tetrahedral coordination environment in **5** and **6** is reflected by  $\tau_4^{[32]}$  and  $\tau_4'^{[33]}$  values of 0.802 and 0.801 for the BPIY adduct and 0.783 as well as 0.762 for the IMPY adduct, respectively. The latter is thus slightly more distorted which may be attributed to the influence of the spatially demanding *tert*-butyl group. When one plane is defined between the Co(II) ion and the TMSA nitrogen atoms on the one hand and another plane created between the central atom and the Lewis base nitrogen atoms, an angle between both planes can be measured that reflects the twist of the Lewis base towards the Co(TMSA)<sub>2</sub> fragment. For **3** - **6**, this angle was found to be the least for **4** (42.95 °) and the largest for **6** (77.01 °), thus directly correlating to the spatial demand of the respective Lewis base (Table 4).

Another aspect in which the four Lewis adducts were compared are their solid state packing and short contacts, whereby latter are defined as distances between individual atoms of different molecules smaller than the sum of their van der Waals radii. Thus, they may indicate weak intermolecular interactions. Graphical illustrations for the packing of **3** - **6** are provided in the SI (section 4). Only H–H interactions between hydrogen atoms of proximate Si(CH<sub>3</sub>)<sub>3</sub> were found for **3** while the terminal imine moieties of the DAD ligand were not involved in any kind of interaction. Those H–H interactions appeared to enforce the formation of individual corrugated [Co(TMSA)<sub>2</sub>(DAD)] chains. Surprisingly, no  $\pi$ – $\pi$  interactions of neighboring N,N-dimethylpyridine-2-amines were observed in **4**. Instead, H–H interactions between amine methyl groups and Si(CH<sub>3</sub>)<sub>3</sub> moieties of TMSA ligands as well as interactions of aromatic hydrogen atoms of pyridine moieties again with Si(CH<sub>3</sub>)<sub>3</sub> groups were monitored. These interactions allowed to establish complanate chains of [Co(TMSA)<sub>2</sub>(DMAPY)] molecules. The solid state packing of **5** presented [Co(TMSA)<sub>2</sub>(BPY)] molecules that were located in a staggered fashion to one another so that a strong overlap of BPY fragments was prevented. Rather, interactions of single aromatic hydrogen atoms with a proximate  $\pi$  system (~3.4 Å - 3.8 Å) were seen. Furthermore, C–H and H–H interactions of aromatic hydrogens with CH<sub>3</sub> groups of nearby TMSA groups contributed to an overall periodic zigzag pattern of molecular chains that were strongly interconnected with one another. Alignment of [Co(TMSA)<sub>2</sub>(IMPY)] molecules to zigzag chains through non-covalent C–H and H–H interactions was noticed in the solid state packing of **6** as well. Contrasting the packing in **5** however, strongly overlapping orientation of proximate pyridine rings facilitated more direct  $\pi$ – $\pi$  interactions (~3.6 Å – 4.0 Å). The cobaltate salt [Co(TMADS)<sub>3</sub>Li(DAD)<sub>2</sub>] (**7**) was constituted of a trigonal planar Co(TMADS)<sub>3</sub><sup>–</sup> anion and a distorted tetrahedral Li(DAD)<sub>2</sub><sup>+</sup> cation as illustrated by **Figure 3**. Exhibiting Li–N bond distances ranging between 2.0492(53) Å and 2.0673(52) Å as well as a  $\tau_4$  value of 0.778 (**Table 5**), the Li(DAD)<sub>2</sub><sup>+</sup> moiety strongly resembled what had prior been reported by Gardiner and co-workers for the cation (average Li–N bond = 2.078 Å,  $\tau_4$  = 0.792). Just as in the case of Gardiner, N–C and C–C bond lengths such as N6–C4 = 1.2704(38) Å and C3–C4 = 1.4882(43) Å indicated the neutral character of the two DAD ligands. Within the Co(TMADS)<sub>3</sub><sup>–</sup> anion, the three ligands spanned around the Co(II) central ion with  $\Sigma^0$  = 359.97(7). The average Co–N bond length of 1.94 Å was found to be located between those observed in homoleptic [Co(TMADS)<sub>2</sub>]<sub>2</sub> (**2**) for terminally coordinating TMADS ligands (1.8907(7) Å) and bridging TMADS ligands (1.9957(8) Å).



**Figure 3:** Solid state structures of  $[\text{Co}(\text{TMADS})_3\text{Li}(\text{DAD})_2]$  (**7**) drawn with thermal ellipsoids at 50 % probability level. Hydrogens are omitted for clarity. On the left, the  $\text{Li}(\text{DAD})_2^+$  cation is depicted while the  $\text{Co}(\text{TMADS})_3^-$  anion is shown on the right.

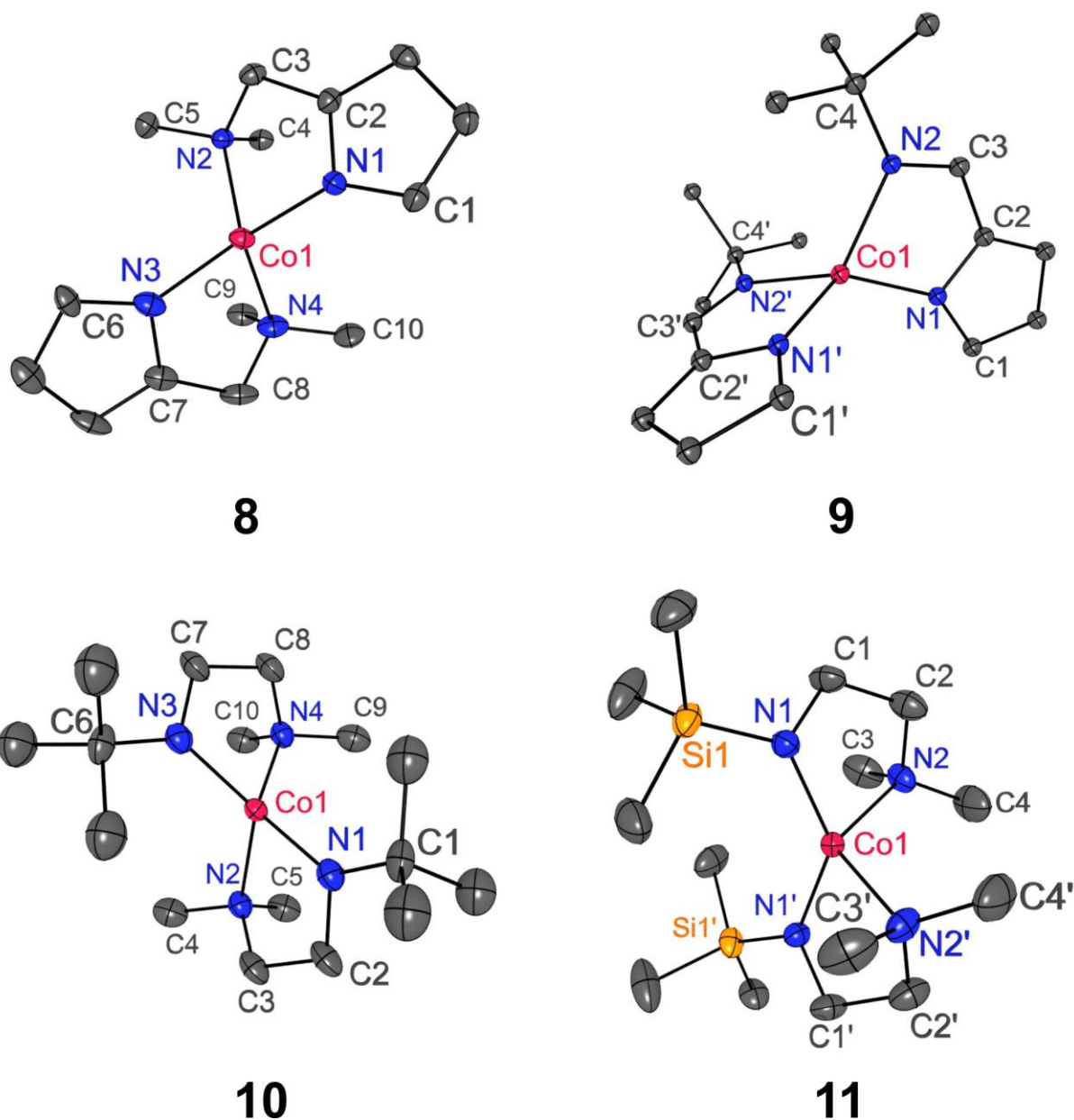
Furthermore, the average N–Si bond lengths within the silylamide ligands was found to be slightly shorter with 1.70 Å (**Table 5**) in comparison to average bond distances of 1.74 Å up to 1.78 Å in terminal and bridging TMADS ligands of **2**. In accordance to that, the Si–N–Si bond angles such as Si1–N1–Si2 with 111.659(130) ° were broadened for a couple of degrees benchmarked to values of 107.927(40) ° and 105.390(39) found for the respective angles in parental **2**. Arguably, the shorter N–Si bond lengths and the widening of the Si–N–Si bond angles can be seen as a necessary adoption to fit three of the TMADS ligands around the central Co(II) ion. Another adoption was observed in the ligand backbone: The absolute values of the dihedral Si–C–C–Si angle amounted to around 36.4 ° and thus became around 5 ° larger compared to the average 31.6 ° found for dihedral Si–C–C–Si angles in **2**. Title compounds **8** - **11**, whose solid state structures are depicted in **Figure 4**, all exhibited a four-fold more or less strongly distorted tetrahedral coordination geometry around the respective Co(II) central ion. For the discussion of structural details however, a subdivision of pyrrolyl coordinated complexes **8** and **9** on the one hand and amido-amino coordinated complexes **10** and **11** on the other, was consequential. The Co1–N1 bond distance between the pyrrolyl nitrogen in amino pyrrolyl complex **7**,  $\text{Co}(\text{AMPR})_2$ , was found to be 1.9568(45) Å and thus slightly shorter than the respective bond in imino pyrrolyl compound **9**,  $\text{Co}(\text{IMPR})_2$ , (1.9813(16) Å, see **Table 6**). In compensation herewith, the opposite observation was made for the Co1–N2 bond distances being 2.0891(45) Å for **8** and 2.0652(19) Å for **9**.

**Table 5:** Selected Interatomic Distances and Angles of compound **7**.

<b>7 [Co(TMADS)<sub>3</sub>Li(DAD)<sub>2</sub>]</b>			
Bond Lengths / Interatomic Distances (Å)			
Co1–N1	1.9410(25)	N3–Si6	1.7100(25)
Co1–N2	1.9428(25)	Li1–N4	2.0658(53)
Co1–N3	1.9415(26)	Li1–N5	2.0499(51)
N1–Si1	1.7063(23)	Li1–N6	2.0492(53)
N1–Si2	1.7041(25)	Li1–N7	2.0673(52)
N2–Si3	1.7080(23)	N6–C4	1.2704(38)
N2–Si4	1.7031(25)	C1–C2	1.5502(25)
N3–Si5	1.7041(25)	C3–C4	1.4882(43)
Angles (°)			
N1–Co1–N2	120.305(102)	N4–Li1–N5	84.611(195)
N2–Co1–N3	117.449(104)	N4–Li1–N6	122.440(250)
N3–Co1–N1	122.216(107)	N4–Li1–N7	127.908(243)
Si1–N1–Si2	111.659(130)	N5–Li1–N6	121.488(249)
Si3–N2–Si4	111.389(132)	N5–Li1–N7	121.289(243)
Si5–N3–Si6	111.398(132)	N6–Li1–N7	84.050(198)
Si5–C1–C2–Si6	-36.474(225)	N6–C3–C4–N7	-3.212(436)
$\Sigma^0$ for Co1 (°)		$\tau_4^{[32]} / \tau_4'^{[33]}$ for Li1	
359.97(7)		0.778 / 0.761	

As expected, the amino-carbon bond N2–C3 in **7** (1.5150(63) Å) clearly exceeded the 1.2725(10) Å found for the N2–C3 imino-carbon bond length present in **9**. Another noticeable difference between **8** and **9** in terms of bonding was observed in the ligand backbones where the C2–C3 bond lengths amounted to 1.4871(84) Å (**8**) and 1.4451(13) Å (**9**), respectively. As it can be seen from **Table 6**, not only the bonding distances except from the above discussed ones but also the bond angles in **8** and **9** were found to be very similar which masks to some extent the pronounced structural difference between the two complexes: Lacking a conjugated  $\pi$ -system, the ligand backbone of **8** can only adopt a conjugative binding mode around the Co(II) ion upon severe twisting which results in a dihedral angle N1–C2–C3–N2 of -35.304(666) °. In stark contrast, the N1–C2–C3–N2 dihedral angle in **9** was found to be nearly negligible with 0.321(106) °. The  $\tau_4$  and  $\tau_4'$  values calculated for both pyrrolyl based complexes illustrated the distorted character of the tetrahedral coordination geometries clearly with 0.708 and 0.652 for Co(AMPR)<sub>2</sub> **8** and less pronounced with 0.782 and 0.774 for Co(IMPR)<sub>2</sub> **9**. For the two structurally closely related amido-amino derivatives Co(TBUAEDMA)<sub>2</sub> (**10**) and Co(TMSAEDMA)<sub>2</sub> (**11**), obtainment of solvable SC-XRD data sets was not trivial as mentioned prior. As explicated in the **SI Section 4**, the TBUAEDMA ligands in **10** and the TMSAEDMA ligands in **11** were found in two-fold disorder around the respective Co(II) ions. This disorder may be referred to as fractional superposition, was more present in **10** than in **11** and a structural solution could be found by description of disordered ligands with two parts.





**Figure 4:** Solid state structures of the title compounds  $\text{Co(AMPR)}_2$  (**8**),  $\text{Co(IMPR)}_2$  (**9**),  $\text{Co(TBUAEDMA)}_2$  (**10**) and  $\text{Co(TMSAEDMA)}_2$  (**11**) drawn with thermal ellipsoids at 50 % probability level. Hydrogens are omitted for clarity. The structure of **9** is reproduced from the data provided by Wei.<sup>[21]</sup> For the structure of **10**, the superposition of partially disordered ligands is omitted for clarity.

In the subsequent discussion and in **Table 6** bond lengths and angles for only one part are considered for clarity. The Co1–N1 amide bond lengths were found to be 1.9165(113) Å and 1.9421(33) Å, respectively (**Figure 4**). Interestingly, these bond lengths are shorter than those seen for TMS-amide bond lengths in the heteroleptic, tetrahedral complexes **5** and **6** and rather comparable to TMS-amide bond lengths found in complexes, **1** - **4**, which exhibit tri-coordinated Co(II) ions. The Co1–N2 bonds describing the distance between the Co(II) ions and the chelating dimethyl-amines amounted to 2.1767(114) Å (**10**) and 2.1478(35) Å (**11**) which is longer than the respective distance found in **7**.

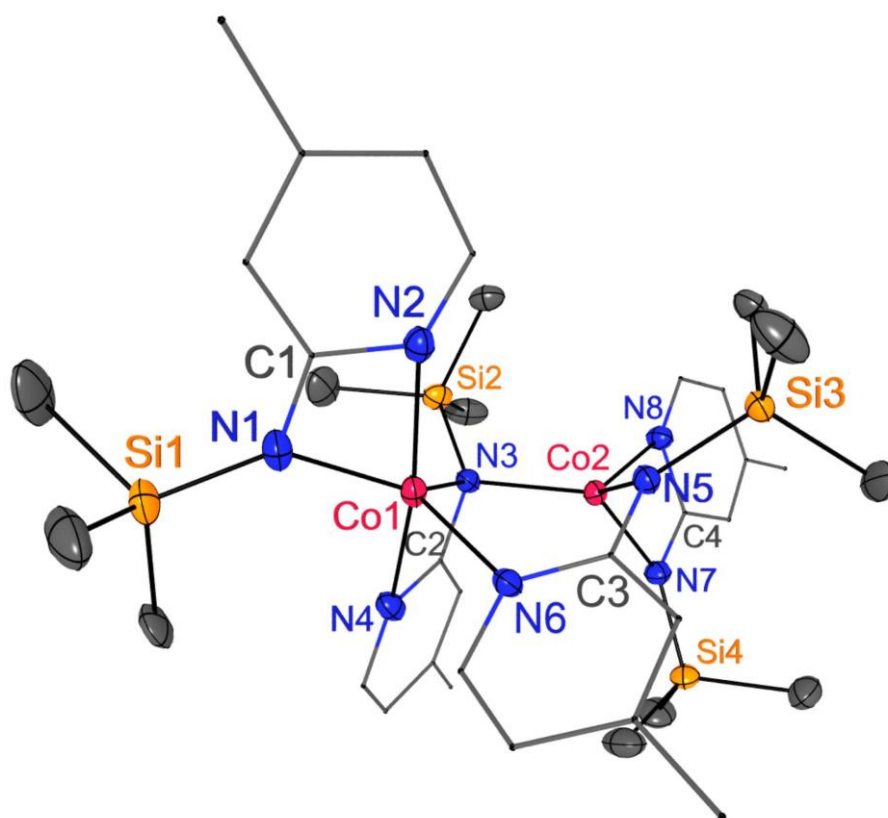
**Table 6:** Selected Bond Lengths, Distances and Angles of Complexes **7**, **8**,<sup>[21]</sup> **9**, and **10**. Abbreviations used for the four complexes in this study are given for clarity.

	<b>8</b> Co(AMPR) <sub>2</sub>	<b>9</b> Co(IMPR) <sub>2</sub>	<b>10</b> Co(TBUAEDMA) <sub>2</sub>	<b>11</b> Co(TMSAEDMA) <sub>2</sub>
Bond Lengths / Interatomic Distances (Å)				
Co1–N1	1.9568(45)	1.9813(16)	1.9165(113)	1.9421(33)
Co1–N2	2.0891(45)	2.0652(19)	2.1767(114)	2.1478(35)
Co1–N3/N1'	1.9551(52)	1.9813(16)	1.8793(107)	1.9421(33)
Co1–N4/N2'	2.1155(46)	2.0652(19)	2.1462(129)	2.1478(35)
N1–Si1	–	–	–	1.6896(37)
N1–C1	1.3557(74)	1.3731(13)	1.4228(200)	1.4751(51)
N1–C2	1.3730(72)	1.3623(14)	1.4768(210)	–
N2–C2	–	–	–	1.4682(59)
N2–C3	1.5150(63)	1.2725(10)	1.4627(202)	1.4680(63)
N2–C4	1.4695(77)	1.4906(14)	1.4874(224)	1.4691(66)
N2–C5	1.4736(80)	–	1.4723(233)	–
C1–C2	–	–	–	1.5405(75)
C2–C3	1.4871(84)	1.4451(13)	1.4873(244)	–
Angles (°)				
N1–Co1–N2	85.236(181)	83.542(39)	83.463(461)	85.946(134)
N1–Co1–N3/N1'	138.692(192)	126.222(47)	130.616(485)	136.736(135)
N1–Co1–N4/N2'	113.400(186)	123.511(46)	125.941(477)	118.723(135)
N2–Co1–N3/N1'	117.933(203)	123.511(46)	127.448(451)	118.723(135)
N2–Co1–N4/N2'	120.325(198)	121.841(46)	105.304(477)	112.451(131)
N3/N1'–Co1–N4/N2'	85.239(193)	83.542(39)	86.105(526)	85.946(134)
C2–C3–N2	109.207(450)	119.572(67)	112.588(1375)	–
C1–N1–Co1	141.379(389)	143.411(59)	111.869(1229)	–
Si1–N1–Co1	–	–	–	116.491(288)
N1–C2–C3–N2	-35.304(666)	0.321(106)	41.893(1876)	–
N1–C1–C2–N2	–	–	–	48.557(487)
$\tau_4^{[32]} / \tau_4'^{[33]}$				
	0.708 / 0.652	0.782 / 0.774	0.723 / 0.713	0.741 / 0.686

With 1.6896(37) Å, the N1–Si1 bond length in **11** was found to be surprisingly short, shorter than *e.g.* N–Si bonds in classic amide compound **1** but expectedly longer than the analogous N1–C1 bond (1.4228(200) Å) in **10**. Both ligand backbones were similarly twisted in terms of the dihedral angles N1–C2–C3–N2 (**10**) and N1–C1–C2–N2 (**11**) that amounted to 41.893(1876) ° and 48.557(487) °, respectively. Furthermore, the  $\tau_4$  and  $\tau_4'$  values for the two amido-amino complexes were determined to be 0.723 and 0.713 for Co(TBUAEDMA)<sub>2</sub> **10** and 0.741 and 0.686 for Co(TMSAEDMA)<sub>2</sub> **11** thus demonstrating a notable degree of distortion in the tetrahedral coordination environments.

As initially stated, the aminopyridinate ligand 4-methyl-N-(trimethylsilyl)pyridine-2-amide, here referred to as TMSMAPY, has found use in the context of Co(II) coordination chemistry prior. Glatz and co-workers, reacted two equivalents of Li-TMSMAPY with CoCl<sub>2</sub> in the presence of 4-*tert*-butylpyridine in THF to obtain an octahedral, mononuclear Co(II) complex, [Co(TMSMAPY)<sub>2</sub>(TBUPY)<sub>2</sub>], in which the TMSMAPY ligands adopted the expected

chelating binding mode.<sup>[20]</sup> In a prior study Glatz and Kempe had introduced the related N<sup>2</sup>,N<sup>6</sup>-bis(trimethylsilyl)pyridine-2,6-diamide ligand (BTMSAPY) for the complexation of Co(II).<sup>[34]</sup> They obtained a binuclear, symmetrical complex, Co<sub>2</sub>(BTMSAPY)<sub>3</sub>, in which both Co(II) ions were surrounded by a slightly distorted tetrahedral coordination sphere. Hereby, one of three BTMSAPY ligands adopted a  $\mu_2$ -coordination utilizing both side chain amide-nitrogen and the pyridine-nitrogen atoms, while the other two were  $\mu_2$ -coordinating with only one side chain amide-nitrogen and pyridine-nitrogen atom. Reminiscence of these structural features is essential when considering our homoleptic and binuclear complex [Co(TMSMAPY)<sub>2</sub>]<sub>2</sub> (**12**). The solid state structure of complex **12** is depicted in **Figure 5** whereby the pyridine ring carbon atoms thermal ellipsoids have been omitted for clarity and only their connectivity is shown. Most notably, the binuclear complex exhibited one Co(II) ion in a strongly distorted pyramidal coordination environment while the second Co(II) ion was placed in an only slightly distorted tetrahedral coordination sphere. This feature is enabled through the different chelation modes of the four TMSMAPY ligands. While two of the ligands coordinated to one Co(II) ion each in the way earlier observed by Glatz in octahedral, mononuclear [Co(TMSMAPY)<sub>2</sub>(TBUPY)<sub>2</sub>], there was  $\mu_2$ -coordination of another TMSMAPY ligand that resembled the second  $\mu_2$ -bridging seen in Co<sub>2</sub>(BTMSAPY)<sub>3</sub> where the aminopyridinate coordinated with its pyridine-nitrogen to one Co(II) ion and with the amido-nitrogen to the other. In **Figure 4**, these nitrogen atoms are labelled as N5 and N6, respectively. Intriguingly, **12** exhibited an additional  $\mu_2$ -bridging mode however that had not been observed by Glatz and co-workers: The last of the four TMSMAPY ligands coordinated with its pyridine-nitrogen, N4 in **Figure 4**, to one Co(II) ion, while its amido-nitrogen, N3, bridges both Co(II) central ions. Selected interatomic distances and angles for title compound **12** are provided in **Table 6**. The typical Co(II) ion - amido-nitrogen bond length was found to vary between roughly 1.98 Å and 2.00 Å. Contrasting this, the Co–N bond distances for the bridging amido-nitrogen were slightly elongated with values of 2.0677(12) Å (Co1–N3) and 2.0402(14) Å (Co2–N3). These bonds were overall notably shorter than the respective ones in [Co(TMSMAPY)<sub>2</sub>(TBUPY)<sub>2</sub>] where the bond lengths averaged out to 2.21 Å. Similarly, the Co–N bonds involving pyridine-nitrogen atoms were found to be shorter in **12** in comparison to the mononuclear reference complex of Glatz. With 2.0418(14) Å the Co1–N6 bond belonging to the  $\mu_2$ -coordinating TMSMAPY ligand was found to be remarkably short and in the same range as amido-nitrogen Co–N bonds.



**12**

**Figure 5:** Solid state structure of title compound  $[\text{Co}(\text{TMSMAPY})_2]_2$  **12** drawn with thermal ellipsoids at 50 % probability level. Hydrogens are omitted for clarity. Likewise, thermal ellipsoids of pyridine carbon atoms are not depicted to ease perception of the Co(II) central ion coordination environments.

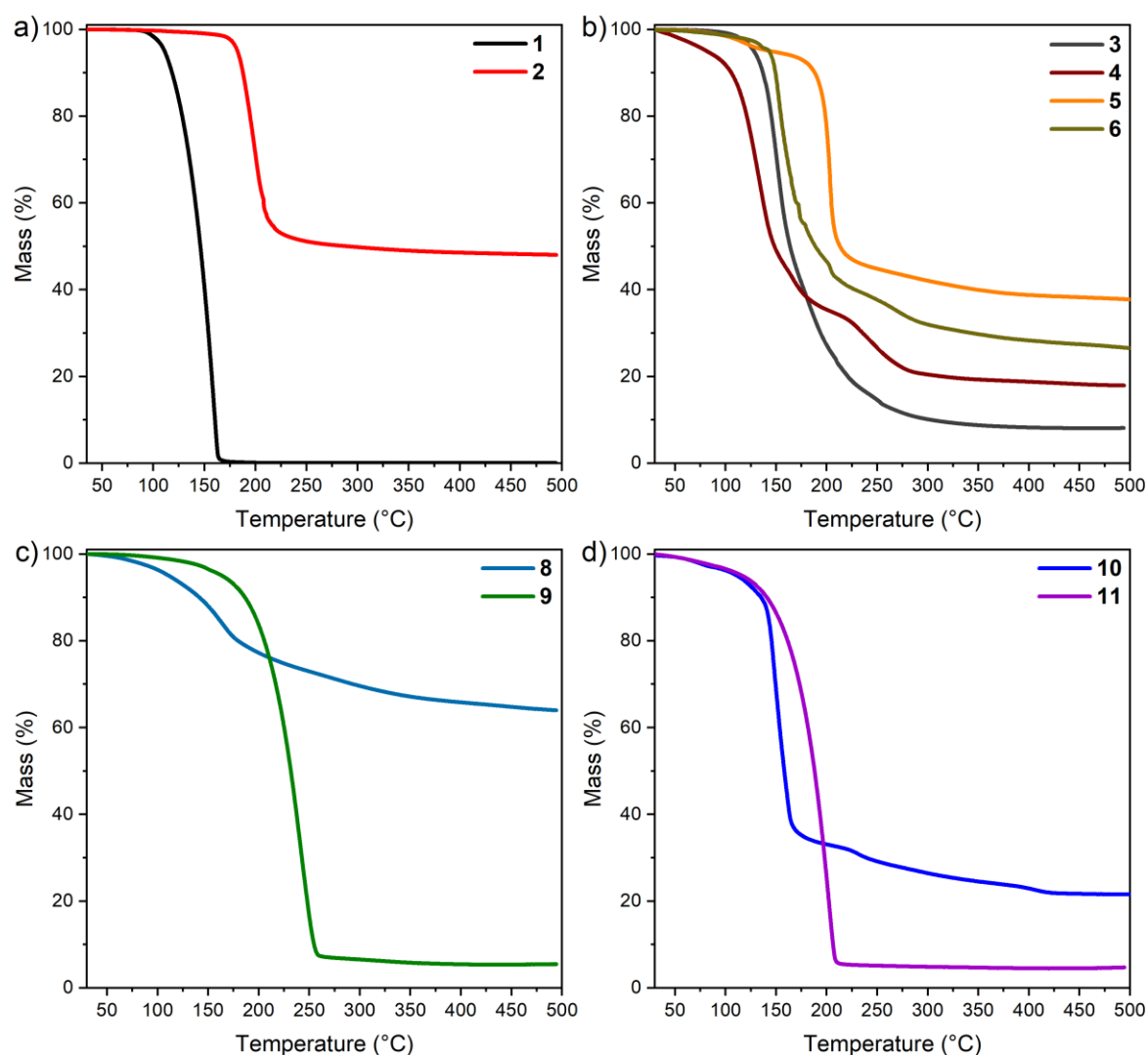
The interatomic Co1–Co2 distance was 2.9531(4) Å and thus distinctly longer than in the dimeric silylamide compounds **1** and **2**. In dependency on the TMSMAPY chelation mode, slight deviations in the bite angles were found in **12**. For those ligands coordinating without bridging, angles N1–Co1–N2 and N7–Co2–N8 were 65.441(51) ° and 66.007(49) ° while the angle N3–Co1–N4, with N3 being the  $\mu_2$ -bridging amido-nitrogen, was slightly narrower (63.761(48) °). The N–C–N ligand spread angle for the fully  $\mu_2$ -bridging TMSMAPY ligand, namely the angle N5–C3–N6, was 117.288(126) ° and thus expectedly larger than the average spread angle of around 112 ° found for the other ligands. Utilizing the angles listed in **Table 7**, the  $\tau_5$  value for central ion Co1 was calculated to be 0.533 while the  $\tau_4$  and  $\tau_4'$  values for ion Co2 were determined to be 0.845 and 0.842. Interestingly, an only minor distorted tetrahedral coordination environment was established around the latter Co(II) ion, potentially on the expense of the coordination environment of the former that found itself right between a square pyramidal and a trigonal bipyramidal coordination geometry.

**Table 7:** Selected Interatomic Distances and Angles of Complexes **12**.

<b>12 [Co(TMSMAPY)<sub>2</sub>]<sub>2</sub></b>			
Bond Lengths / Interatomic Distances (Å)			
Co1–N1	2.0021(14)	Co2–N3	2.0402(14)
Co1–N2	2.1567(13)	Co2–N5	1.9834(13)
Co1–N3	2.0677(12)	Co2–N7	1.9984(13)
Co1–N4	2.2632(13)	Co2–N8	2.1341(12)
Co1–N6	2.0418(14)	Co1---Co2	2.9531(4)
Angles (°)			
N1–Co1–N2	65.441(51)	N3–Co2–N5	120.967(53)
N1–Co1–N3	136.650(52)	N3–Co2–N7	115.739(52)
N1–Co1–N4	109.832(52)	N3–Co2–N8	107.054(49)
N1–Co1–N6	113.610(54)	N5–Co2–N7	114.912(51)
N2–Co1–N3	111.843(48)	N5–Co2–N8	119.874(49)
N2–Co1–N4	168.614(49)	N7–Co2–N8	66.007(49)
N2–Co1–N6	100.754(52)	N1–C1–N2	111.440(135)
N3–Co1–N4	63.761(48)	N3–C2–N4	112.438(125)
N3–Co1–N6	109.385(51)	N5–C3–N6	117.288(126)
N4–Co1–N6	90.629(49)	N7–C4–N8	111.939(128)
$\tau_5^{[35]}$ for Co1		$\tau_4^{[32]} / \tau_4'^{[33]}$ (or Co2)	
0.533		0.845 / 0.842	

**Thermal Properties:**

For the initial assessment of a potential precursor in terms of volatility and thermal stability, thermogravimetric analysis (TGA) is an established procedure. Hereby, a small quantity of a sample is weighted (~10 mg for analytes in this study) and the mass loss as a function of heating temperature is traced. While evaporation of the intact analyte results ideally in the absence of a residual mass, high residual masses indicate early and undesirable decomposition. Title compounds **1** - **12** were subjected to TG experiments to investigate their fundamental volatilization behavior and to draw conclusions on the effect of slight structural differences of related compounds hereon (**Figure 6**). As it can be seen from **Figure 6 a**, the two silylamides **1** and **2** demonstrated considerably different evaporation characteristics. While **1** underwent a sharp single step evaporation process with an onset temperature, here derived by the tangent method, of roughly 128 °C, the onset temperature for **2** was found to be around 181 °C. Additionally, TGA of **1** resulted in a negligible residual mass while the residual mass of **2** was 48 % at 500 °C. As priorly discussed, **2** exhibited a divergent solid state structure in comparison to **1** in which the rigidity of the ligand periphery induced strain on the Co<sub>2</sub>N<sub>2</sub> core structure. Even though the exact mechanism of evaporation for neither **1** nor **2** is known, it appeared manifest that the TMADS ligand in **2** impeded volatilization until a notable fraction of the analyte decomposed. Contrasting this, **1** apparently undergoes a conversion into a volatile and thermally stable product, presumably the monomer, upon heating.



**Figure 6:** Thermogravimetric Analyses (TGA) of **a)** dimeric silylamides [Co(TMSA)<sub>2</sub>]<sub>2</sub> (**1**) and [Co(TMADS)<sub>2</sub>]<sub>2</sub> (**2**); **b)** [Co(TMSA)<sub>2</sub>L] Lewis adducts [Co(TMSA)<sub>2</sub>(DAD)] (**3**), [Co(TMSA)<sub>2</sub>(DMAPY)] (**4**), [Co(TMSA)<sub>2</sub>(BPY)] (**5**) and [Co(TMSA)<sub>2</sub>(IMPY)] (**6**); **c)** pyrrolate-amide Co(AMPR)<sub>2</sub> (**8**) and pyrrolate-imide Co(IMPR)<sub>2</sub> (**9**); **d)** amido-amines Co(TBUAEDMA)<sub>2</sub> (**10**) and Co(TMSAEDMA)<sub>2</sub> (**11**). A heating rate of 10 °C·min<sup>-1</sup> was used for all experiments, and the mass loadings were 10.0 ± 0.1 mg for each sample.

Converting dimeric **1** into monomeric adducts employing the Lewis bases DAD, DMAPY, BPY and IMPY forwarded complexes **3** - **6** that were rendered to possess inferior volatilization characteristics in comparison to the parental complex (**Figure 6 b**). Considering individual residual masses for **3** – **6**, it became evident however that mass loss did not only originate from loss of the respective Lewis base but from volatilization of the intact precursor. Intriguingly, [Co(TMSA)<sub>2</sub>(DAD)] (**3**) with its unusual onefold coordination of the DAD ligand to the Co(II) ion demonstrated the best performance with a residual mass of around 8.1 % and a rather smooth mass loss trend. While Lewis acid base complexation with the chosen Lewis bases failed to yield precursors with improved volatility, they might yet be interesting for CVD

applications as thermal instability is introduced. Besides, the initially mentioned successful demonstration of  $[\text{Co}(\text{TMSA})_2(\text{THF})]$  as ALD precursor for  $\text{CoO}_x$  thin films through Iivonen and co-workers<sup>[10]</sup> still evidences the complexation approach to be viable for the synthesis of enhanced Co(II) ALD precursors. The most pronounced contrast in terms of thermal stability and volatility was observed for the two pyrrolato complexes **8** and **9** as it can be seen in **Figure 6 c**. While the latter demonstrated clean one-step evaporation with a residual mass of only 5.5 % and an onset temperature of around 203 °C, compound **8** with its non- $\pi$ -conjugated pyrrole dimethylaminoethyl side chain barely volatilized intactly. At this stage, the mass loss was fully ascribed to precursor decomposition and release of organic, volatile decomposition products. Bulk sublimation experiments, described in the subsequent section should confirm this initial assessment. Lastly, as illustrated by **Figure 6 d**, amido-amine compound **10** with its *tert*-butyl amido ligand moiety outperformed the trimethylsilyl derivate **11** in terms of volatilization onset (140 °C vs. 169 °C) but showed inferior thermal stability evidenced by a notably higher residual mass (21.6 % vs. 4.7 %). Dimeric compound **12** was subjected to TGA as well and the experimental data can be found in the SI. Unsurprisingly, the mass loss was found to be dominated by a multitude of overlapping decomposition events with no evidence for partial intact precursor evaporation which rendered **12** to be the least suitable CVD/ALD precursor candidate.

While TGA is a most valuable tool to initially assess the performance of a precursor candidate, it can be deceptive as the evaporation conditions typically differ from evaporation parameters applied to precursors in CVD and ALD processes. More precisely, TGA only probes a few milligrams of an analyte at atmospheric pressure and not multi-gram quantities under roughing pump vacuum conditions. Additionally, the adjustment of carrier gas flows can have a strong impact on the observed volatilization behavior. Consequently, we probed compounds **1** - **12** under more realistic process conditions: 300 mg of each compound were subjected to sublimation at around  $1 \times 10^{-1}$  mbar at the lowest temperature at which sublimation was observed. The recovered substances were first weighted and then subjected to elemental analysis (EA) to assess their purity compared to non-sublimed reference samples. **Table 8** summarizes the respective sublimation temperatures  $T_s$  and the bulk sublimation recovery yields alongside the residual masses from TGA and melting points  $T_M$  obtained from melting point measurements. Expectedly, compounds **1**, **9** and **11** which had already demonstrated the best performance in TGA were recovered with high yields ranging from 78 % (**9**) up to over 90 % (**1**, **11**), whereby the recovered substances EA did not differ from the reference samples (difference in C, H and N content in % smaller than 0.3 %).

**Table 8:** Thermal properties of title compounds **1** - **12** derived from melting point measurements, TGA and bulk sublimation experiments. Being a salt with strong ionic interactions, **7** was excluded from the study.

Compound	T <sub>M</sub> (°C)	Residual mass (%)	T <sub>S</sub> (°C) <sup>a</sup>	Bulk Sublimation Recovery (%) <sup>a</sup>
<b>1</b>	89	0.1	70	93.7
<b>2</b>	205	48.0	110	30.3
<b>3</b>	99	8.1	80	48.2
<b>4</b>	78	17.9	75	62.0
<b>5</b>	152	37.7	— <sup>b</sup>	— <sup>b</sup>
<b>6</b>	141	26.7	100	17.5
<b>8</b>	223	64.0	— <sup>b</sup>	— <sup>b</sup>
<b>9</b>	155	5.5	110	78.4
<b>10</b>	84	21.6	80	35.2
<b>11</b>	90	4.7	80	92.2
<b>12</b>	85	25.8	— <sup>b</sup>	— <sup>b</sup>

<sup>a</sup>Quantities of 300 mg of the compounds were filled into Schlenk flasks with attached sublimation fingers and sublimed at given T<sub>S</sub> in vacuum (1 x 10<sup>-1</sup> mbar). <sup>b</sup>Determination not possible prior to decomposition of the sample.

Likewise, recovered material from compounds **3** and **4** was found to be pure by EA. However, the recovery rates were already significantly lower with around 50 % and 60 % and decomposed material was observed at the bottom of the sublimation set-up. Compounds **2**, **6** and **10** were sublimed with low recovery yields and only for **10** the conducted EA was found to not significantly differ from the reference. Samples of **5**, **8** and **12** could not be recovered by sublimation as decomposition occurred upon careful and stepwise heat-up to a maximum sublimation temperature of 120 °C. In summary, the suitability of candidates **1**, **9** and **11** for CVD as well as ALD applications in terms of their fundamental thermal properties was validated while the sublimation experiments allowed to identify **3** and **4** more clearly as potential CVD precursors. A significant advantage of candidate **9** over all other competitors of the investigated compound series is the absence of silicon in the ligand sphere which render it more appealing for process implementation as *e.g.* the contamination of metallic cobalt thin films by silicon is unwanted in semiconductor industry.<sup>[36]</sup>

## Conclusions:

Conclusively, a series of Co(II) (silyl)amides and Lewis adducts thereof as well as Co(II) pyrrolates and aminopyridinates was synthesized. The in total 12 complexes were classified based on their structural features which allowed a detailed discussion and cross-comparison of their solid-state structures. While the DAD ligand in Lewis adduct [Co(TMSA)<sub>2</sub>(DAD)] adopted an unusual non-chelating bonding mode, the dimeric aminopyridinate [Co(TMSMAPY)<sub>2</sub>]<sub>2</sub> was found to exhibit the most intriguing structural properties, namely one Co(II) ion surrounded by a slightly distorted tetrahedral coordination environment and the other placed in a strongly distorted trigonal bipyramidal coordination. Thermal property assessment by complementary TGA and bulk sublimation experiments allowed to identify the well-known



[Co(TMSA)<sub>2</sub>]<sub>2</sub> as a suitable precursor alongside the similarly well-performing monomeric Co(IMPR)<sub>2</sub> and Co(TMSAEDMA)<sub>2</sub>. Hereby, Co(II) complexes of the imido-pyrrolato class render a promising and versatile precursor family worth to be looked into in more detail. Rational variation of the imido-nitrogen alkyl side chain may allow to selectively alter the physico-chemical properties of the resulting Co(II) complexes so that *e.g.* the melting point may be reduced and the volatility increased while the overall high thermal stability is maintained.

## ASSOCIATED CONTENT

TGA plots and IR spectra for all compounds discussed in this study.

### Accession Codes

CCDC 2092887, 209288, 2094912 - 2094918 contain the supplementary crystallographic data for this paper. These data can be obtained free of charge via [www.ccdc.cam.ac.uk/data\\_request/cif](http://www.ccdc.cam.ac.uk/data_request/cif), or by emailing [data\\_request@ccdc.cam.ac.uk](mailto:data_request@ccdc.cam.ac.uk), or by contacting The Cambridge Crystallographic Data Centre, 12 Union Road, Cambridge CB2 1EZ, UK; fax: +44 1223 336033.

## AUTHOR INFORMATION

### Corresponding Author

\*[anjana.devi@rub.de](mailto:anjana.devi@rub.de)

### Author Contributions

The manuscript was written through contributions of all authors. All authors have given approval to the final version of the manuscript. <sup>†</sup>N. Boysen and M. Land contributed to this manuscript equally.

## ACKNOWLEDGMENT

D.Z. thanks the German Academic Exchange Service (DAAD-1-year fellow program) and the Fond of Chemical Industries (Kekulé fellowship) for ideational and financial support. M.A.L thanks the Natural Sciences and Engineering Research Council of Canada (NSERC) for financial support through the Canada Graduate Scholarship Program (CGS-D).

## Experimental section: EA

### General methods and procedures:

All manipulations were performed under air-free conditions under dried Ar atmosphere using conventional Schlenk techniques or in a Ar/N<sub>2</sub>-filled (AirLiquide, 99.998% purity) MBraun Labmaster 120/130 dryboxes. Solvents were purified by an MBraun-SPS-800 purification system and stored over 4 Å molecular sieves for more than a day before use. Deuterated benzene (C<sub>6</sub>D<sub>6</sub>) was purchased from Millipore and degassed by freeze-pump procedure prior to use. Reagents listed hereafter have been purchased from Sigma Aldrich and were used as received if not stated differently. Abbreviations enclosed in brackets indicate acronyms of the ligands that have been used in this study:

CoCl<sub>2</sub> (anhydrous 99.9 %), N,N-bis(trimethylsilyl)amine (H-TMSA) (99.5 %), 2,2,5,5-tetramethyl-1,2,5-azadisilolidine (H-TMADS) [Gelest Inc. (99.5 %), <sup>n</sup>BuLi (2.0 M in hexanes) and *tert*-butylamine (99.5 %), trimethylsilyl-chloride (99.0%), glyoxal solution in water (40 wt. %), 2,2-bipyridine (99.0%) (BPY) , 2-pyridinecarboxaldehyde (99.5 %), N,N-dimethylpyridine-2-amine (99.0 %) (DMAPY), 2-amino-4-picoline (99.0 %), pyrrole (99.0 %), 2-pyrrolicarboxaldehyde (99.0 %), N,N-dimethylethylene-diamine (97.0 %, freshly distilled prior to use) and 2-chloro-N,N-dimethylethylen hydrochloride (98.0 %).

Utilizing the reagents above, the ligands listed in the following have been synthesized according to literature reported procedures. Prior to use, their purity was assessed by <sup>1</sup>H-NMR spectroscopy: N,N'-di-*tert*-butylethane-1,2-diimine (DAD),<sup>[37]</sup> N-*tert*-butyl-1-(pyridine-2-yl)methanimine (IMPY),<sup>[38]</sup> 4-methyl-N-(trimethylsilyl)pyridine-2-amine (H-TMSAPY),<sup>[30]</sup> N,N-dimethyl-1-(1H-pyrrol-2-yl)methanamine (H-AMPR),<sup>[39]</sup> N-*tert*-butyl-1-(1H-pyrrol-2-yl)methanimine (H-IMPR),<sup>[40]</sup> N,N-dimethyl(N'-*tert*-butyl)ethane-1,2-diamine (H-TBUAEDMA),<sup>[27]</sup> N,N-dimethyl(N'-trimethylsilyl)ethane-1,2-diamine (H-TMSAEDMA)<sup>[28]</sup>.

<sup>1</sup>H Nuclear Magnetic Resonance (NMR) spectra for magnetic moment estimations based on the Evans<sup>[23]</sup> method were recorded on Bruker Avance II 300 MHz instruments. Electron impact mass spectrometry (EI-MS) was either performed with a Kratos Concept - Magnetic sector Electron impact mass spectrometer or with a Varian MAT spectrometer in high resolution mode. Elemental analysis was conducted with a vario micro cube elemental analysis tool (Elementar Analysensysteme) in CHNS analysis mode. IR spectroscopic measurements were performed on a Perkin Elmer Spectrum Two with the UATR Two diamond crystal device operated in an MBraun drybox. TGA was performed on Pt pans with a TA Instruments Q500 housed in an

MBraun Labmaster 130 dry-box filled with nitrogen gas (99.998 % purity). Pt pans were cleaned by sequential ultrasonication in dilute nitric acid (~3 N), water, then 2-propanol. They were then heated until red hot by a propane torch flame in air to remove any remaining impurities. Experiments were performed under a flow of ultrapure nitrogen (99.999 % purity, 6 sccm) at 10 °C min<sup>-1</sup> to a maximum temperature of 500 °C with mass loadings of ~10 mg. For bulk sublimation experiments, a sublimation set-up consisting of a Schlenk flask, and a cooling finger was heated out under vacuum and subsequently charged with 300 mg of the respective analyte before the sublimation experiment was started. For the benefit of consistency, the same set-up was used for all compounds.

#### Bis(bis(trimethylsilylamido)cobalt(II)) (1)

Modifying a procedure described by Bryan,<sup>[11]</sup> a Schlenk flask was charged with 7.24 g (30 mmol) of prior prepared and isolated Li-TMSA·Et<sub>2</sub>O adduct as well as 2.07 g (16 mmol) of CoCl<sub>2</sub>. To this neat reactant mixture 80 ml of Et<sub>2</sub>O were added. The initial blue suspension quickly colorized to dark grey. Upon refluxing at 45 °C for 12 h the suspension adopted a dark green color. Et<sub>2</sub>O was removed under reduced pressure and the crude product extracted with 3 x 20 ml of pentane via cannula filtration. Removal of the solvent under reduced pressure yielded a dark green semisolid product that was distilled in vacuum at 90 °C in a simple flask-to-flask apparatus whereby the receiver flask was cooled with dry ice. **1** solidified in the receiver flask upon cooling as dichroic green to red substance that was redissolved in pentane and recrystallized at -30 °C to afford dark red crystals. Alternatively, the target compound can directly be sublimed onto a sublimation finger within a couple of hours at 65 °C. Yields: 4.23 g - 4.51 g (74 % - 79 %). **1** : Dark red solid, m.p. 89 °C. Sublimation: 65 °C (1 x 10<sup>-1</sup> mbar). **HRMS (EI)** for the molecular ion peak [M<sub>mono</sub>]<sup>+</sup> for the monomer: Found, m/z = 379.1351, calcd. 379.1288. **IR** in ATR mode:  $\nu$  (cm<sup>-1</sup>) = 2950.7 (m), 2895.1 (m), 1431.5 (w), 1388.2 (w), 1244.3 (s), 1186.3 (w), 1150.2 (w), 1088.0 (w), 1044.8 (m), 977.1 (s), 916.8 (s), 820.9 (s), 789.3 (s), 775.5 (s), 752.5 (s), 716.5 (s), 663.3 (s), 632.3 (s), 611.5 (s), 551.8 (m). **EA** calcd. (%): C 37.96, H 9.56, N 7.38; found (%): C 38.23, H 9.67, N 7.44.  $\mu_B$  in C<sub>6</sub>D<sub>6</sub> solution = 5.56 (Evans' method).

#### Bis(bis(2,2,5,5-tetramethyl-1,2,5-azadisilolidinyl)cobalt(II)) (2)

1.92 g (12 mmol) of H-TMADS were diluted in 50 ml of Et<sub>2</sub>O and 6 ml of a 2 M <sup>n</sup>BuLi solution in hexanes were added dropwise. After stirring for 1 h, the resulting solution was transferred to an Et<sub>2</sub>O slurry (40 ml) of 0.78 g (6 mmol) of CoCl<sub>2</sub> dropwise over the course of 5 minutes. As for **1**, a rapid color change of the slurry from blue to dark grey was observed that changed to

dark red upon refluxing at 45 °C for 12 h. The solvent was removed under reduced pressure, the crude product extracted with 3 x 20 ml pentane and filtered through a glass filter column charged with celite. Solvent removal yielded the crude product as dark red to black waxy solid. Flask-to-flask distillation (100 °C) as described for **1** forwarded **2** as dark red-black solid that formed SC-XRD quality needles upon recrystallization at -30 °C from pentane. Concomitant decomposition during distillation was more pronounced than for **1** decreasing the yield to 0.85 g (38 %). **2** : Dark red/black solid, m.p. 205 °C. Sublimation: 110 °C (1 x 10<sup>-1</sup> mbar). **HRMS (EI)** for the molecular ion peak [M<sub>mono</sub>]<sup>+</sup> for the monomer: Found, m/z = 375.7739, calcd. 375.6752. **IR** in ATR mode:  $\nu$  (cm<sup>-1</sup>) = 2953.0 (m), 2899.2 (m), 2791.6 (w), 1462.5 (w), 1414.0 (m), 1244.0 (s), 1198.2 (m), 1093.2 (m), 1017.5 (s), 946.6 (m), 867.3 (s), 846.7 (s), 837.6 (s), 814.5 (s), 785.5 (s), 768.6 (s), 672.2 (s), 658.9 (s), 621.4 (s). **EA** calcd. (%): C 38.27, H 8.59, N 7.46; found (%): C 38.72, H 8.42, N 7.37.  $\mu_B$  in C<sub>6</sub>D<sub>6</sub> solution = 5.32 (Evans' method).

#### Bis(trimethylsilylamido)cobalt(II) N,N'-di-*tert*-butylethane-1,2-diimine adduct (**3**)

N,N'-di-*tert*-butylethane-1,2-diimine (0.4 g, 2 mmol) was dissolved in 20 ml of pentane and the solution added at room temperature to a pentane (15ml) suspension of **1** (0.78 g, 2 mmol). The initial dark green to yellow suspension brightened up to a clear green upon stirring for 30 minutes. Stirring was continued for additional 2 h before the solvent was removed under reduced pressure until the formation of bright green crystallites was observed. At this point, the reaction solution was allowed to warm up to room temperature again to redissolve the formed solids. Storage of the solution overnight at -30 °C afforded **3** as bright green crystals. Yield: 0.91 g (83 %). **3** : bright green solid, m.p. 99 °C. Sublimation: 80 °C (1 x 10<sup>-1</sup> mbar). **HRMS (EI)** for the molecular ion peak [M]<sup>+</sup>: Found, m/z = 547.2632, calcd. 547.2914. **IR** in ATR mode:  $\nu$  (cm<sup>-1</sup>) = 2964.9 (m), 2947.6 (m), 2895.3 (w), 1631.9 (w), 1606.1 (w), 1474.9 (w), 1434.0 (w), 1396.7 (w), 1367.3 (w), 1310.2 (w), 1255.7 (m), 1240.3 (s), 1211.3 (w), 1192.3 (w), 1094.3 (m), 1017.2 (m), 952.0 (s), 846.8 (s), 826.0 (s), 812.4 (s), 784.3 (s), 748.1 (s), 708.2 (m), 665.5 (s), 629.3 (m), 623.9 (m), 611.2 (m). **EA** calcd. (%): C 47.33, H 10.02, N 10.51; found (%): C 47.92, H 9.93, N 10.43.  $\mu_B$  in C<sub>6</sub>D<sub>6</sub> solution = 4.26 (Evans' method).

#### Bis(trimethylsilylamido)cobalt(II) N,N-dimethylpyridine-2-amine adduct (**4**)

Following the procedure described for **3**, 0.78 g (2 mmol) of **1** were reacted with 0.24 g (2 mmol) of N,N-dimethylpyridine-2-amine in pentane. Upon storage at -30 °C in a freezer overnight, **4** was isolated from a concentrated pentane solution as green, extremely air and moisture sensitive crystals. Yield: 0.76 g (76 %). **4** : green solid, m.p. 78 °C. Sublimation: 75 °C (1 x 10<sup>-1</sup> mbar). **HRMS (EI)** for the molecular ion peak [M]<sup>+</sup>: Found, m/z = 501.1876, calcd.

501.2132. **IR** in ATR mode:  $\nu$  (cm<sup>-1</sup>) = 2946.7 (m), 2893.1 (m), 2818.3 (w), 1616.5 (m), 1554.2 (m), 1522.5 (m), 1455.9 (w), 1432.7 (m), 1408.7 (m), 1378.6 (m), 1321.0 (m), 1253.2 (m), 1239.4 (s), 1179.5 (m), 1171.6 (m), 1097.9 (w), 1065.4 (w), 998.6 (m), 958.2 (s), 883.5 (s), 842.2 (s), 814.8 (s), 783.2 (s), 769.4 (s), 751.9 (s), 734.2 (s), 707.6 (m), 665.4 (s), 634.9 (m), 629.9 (m), 610.2 (s), 526.7 (m). **EA** calcd. (%): C 45.47, H 9.24, N 11.16; found (%): C 44.62, H 9.06, N 11.28.  $\mu_B$  in C<sub>6</sub>D<sub>6</sub> solution = 4.75 (Evans' method).

Bis(trimethylsilylamido)cobalt(II) 2,2'-bipyridine adduct (5)

Following the procedure described for **3**, 0.78 g (2 mmol) of **1** were reacted with 0.31 g (2 mmol) of 2,2'-bipyridine in pentane. A red solution was obtained, which was concentrated and stored at -30 °C in a freezer overnight. **5** was isolated from this solution as red crystalline solid. Yield: 0.93 g (87 %). **5** : red solid, m.p. 152 °C. Sublimation: not successful. **HRMS (EI)** for the molecular ion peak [M]<sup>+</sup>: Found, m/z = not detected, calcd. 535.1975. **IR** in ATR mode:  $\nu$  (cm<sup>-1</sup>) = 2962.9 (w), 2909.3 (w), 2891.3 (w), 2879.7 (w), 2789.4 (w), 1652.8 (w), 1632.6 (w), 1599.7 (w), 1571.7 (w), 1474.8 (w), 1416.2 (w), 1395.5 (w), 1382.9 (w), 1365.3 (w), 1334.7 (w), 1259.9 (m), 1241.7 (m), 1198.9 (w), 1092.9 (m), 1012.4 (m), 978.9 (m), 947.4 (m), 882.2 (s), 858.8 (s), 798.6 (s), 773.2 (s), 663.1 (m), 646.0 (m), 620.3 (m). **EA** calcd. (%): C 49.31, H 8.28, N 10.46; found (%): C 49.76, H 8.13, N 10.21.  $\mu_B$  in C<sub>6</sub>D<sub>6</sub> solution = 4.49 (Evans' method).

Bis(trimethylsilylamido)cobalt(II) N-tert-butyl-1-(pyridin-2-yl)methane-imine adduct (6)

Following the procedure described for **3**, 0.78 g (2 mmol) of **1** were reacted with 0.32 g (2 mmol) of N-tert-butyl-1-(pyridin-2-yl)methanimine in pentane to yield a brown-yellow solution. Partial solvent removal and storage at -30 °C overnight afforded **6** as brown-red crystals. Yield: 0.86 g (80 %). **6** : brown solid, m.p. 141 °C. Sublimation: 100 °C (1 x 10<sup>-1</sup> mbar). **HRMS (EI)** for the molecular ion peak [M]<sup>+</sup>: Found, m/z = 541.2338, calcd. 541.2445. **IR** in ATR mode:  $\nu$  (cm<sup>-1</sup>) = 2970.1 (w), 2943.6 (m), 2894.1 (w), 1634.0 (w), 1593.3 (m), 1568.7 (w), 1478.1 (w), 1433.2 (w), 1395.9 (w), 1375.2 (w), 1362.8 (w), 1303.2 (w), 1256.6 (m), 1243.9 (m), 1231.8 (m), 1196.5 (m), 1155.8 (w), 1104.7 (w), 1050.9 (w), 1030.3 (w), 1015.0 (w), 960.1 (s), 920.0 (m), 884.8 (m), 861.3 (s), 840.7 (s), 820.1 (s), 776.1 (s), 770.4 (s), 744.8 (s), 716.4 (m), 704.4 (m), 659.6 (s), 634.7 (m), 612.7 (m). **EA** calcd. (%): C 48.76, H 9.30, N 10.34; found (%): C 48.43, H 9.28, N 10.43.  $\mu_B$  in C<sub>6</sub>D<sub>6</sub> solution = 4.36 (Evans' method).

Tris(2,2,5,5-tetramethyl-1,2,5-azadisilolidinyl)cobaltate(II) bis(N,N'-di-tert-butylethane-1,2-diimine)lithium(I) (7)

The salt  $[\text{Co}(\text{TMADS})_3\text{Li}(\text{DAD})_2]$  was obtained from the *in-situ* reaction of freshly prepared  $[\text{Co}(\text{TMADS})_2]_2$  in etheric solution in the presence of partly dissolved LiCl upon addition of DAD. First, 956 mg (6 mmol) of H-TMADS were diluted in 30 ml of  $\text{Et}_2\text{O}$  and cooled with an ice bath to 0 °C before 3.75 ml of a 1.6 M  $n\text{BuLi}$  solution were added. The mixture was allowed to warm up to RT and stirred for 1 y, 672 mg (4 mmol) of DAD were added to the solution and stirring was continued for 6 h at RT. The solvent was removed in vacuum with mild heating (40 °C) and the dark red crude product extracted with pentane. The resulting solution was filtered, concentrated and stored in a freezer to yield 764 mg (yield: 58.0 %) of dark red crystals. **7** : dark red solid, Sublimation: not possible. **HRMS (EI)** for the molecular ion peak  $[\text{M}]^+$ : Calcd. 876.5209 but not detected. **IR** in ATR mode:  $\nu$  ( $\text{cm}^{-1}$ ) = 2962.9 (w), 2909.3 (w), 2891.3 (w), 2879.7 (w), 2789.4 (w), 1652.8 (w), 1632.6 (w), 1599.7 (w), 1571.7 (w), 1474.8 (w), 1416.2 (w), 1395.5 (w), 1382.9 (w), 1365.3 (w), 1334.7 (w), 1259.9 (m), 1241.7 (m), 1198.8 (w), 1092.9 (m), 1012.0 (m), 978.9 (m), 947.4 (m), 882.2 (s), 858.9 (s), 798.6 (s), 773.2 (s), 663.1 (m), 646.0 (m), 620.3 (m). **EA** calcd (%): C 52.01, H 10.11, N 11.17; found (%): C 51.15, H 10.23, N 11.32.  $\mu_{\text{B}}$  in  $\text{C}_6\text{D}_6$  solution = 5.01 (Evans' method).

#### Bis[N,N'-2-(dimethylaminomethyl)pyrrolyl]cobalt(II) (**8**)

40 ml of  $\text{Et}_2\text{O}$  were added to 1.89 g (5 mmol) of **1** to obtain a suspension. In parallel 1.24 g (10 mmol) of N,N'-2-(dimethylaminomethyl)pyrrole were dissolved in 40 ml of  $\text{Et}_2\text{O}$  and added to the suspension of **1** by cannula transfer. The resulting reaction mixture was refluxed at 45 °C for 12 h. With proceeding reaction time precipitation of a red-brown solid, precipitated **8**, was observed. The solution was subsequently separated from precipitated **8** via filtration and stored at -30 °C to yield SC-XRD quality crystals of **8**. The precipitate was dried under reduced pressure. Elemental analysis of both product fractions was nearly congruent and in accordance with the expected product. The combined yield amounted to 1.13 g (74 %). **8** : red-brown solid, m.p. 223 °C. Sublimation: not possible. **HRMS (EI)** for the molecular ion peak  $[\text{M}]^+$ : Found,  $m/z = 305.0419$ , calcd. 305.1176. **IR** in ATR mode:  $\nu$  ( $\text{cm}^{-1}$ ) = 3327.2 (w), 3104.6 (w), 2985.7 (w), 2962.0 (w), 2896.2 (w), 2874.4 (w), 2843.2 (w), 2800.9 (w), 1602.5 (w), 1458.3 (m), 1441.8 (m), 1399.6 (m), 1348.2 (w), 1302.1 (w), 1278.4 (w), 1262.5 (m), 1224.2 (m), 1187.5 (m), 1166.4 (m), 1137.2 (m), 1100.5 (m), 1062.2 (w), 1022.6 (m), 967.3 (m), 898.8 (w), 884.2 (w), 838.1 (m), 798.5 (m), 769.7 (m), 761.0 (m), 746.1 (m), 725.3 (s), 709.6 (s), 653.0 (m), 618.9 (m). **EA** calcd. (%): C 55.08, H 7.26, N 18.35; found (%): C 54.81, H 7.11, N 18.77.  $\mu_{\text{B}}$  in  $\text{C}_6\text{D}_6$  solution = 4.40 (Evans' method).

#### Bis(N-2-(tert-butyliminomethyl)pyrrolyl)cobalt(II) (**9**)

Similarly to the procedure described for **8**, 1.49 g (10 mmol) of N-2-(*tert*-butyliminomethyl)pyrrole dissolved in 40 ml of Et<sub>2</sub>O were added via cannula to a slurry of 1.89 g (5 mmol) of **1** in 60 ml Et<sub>2</sub>O. The reaction mixture was stirred and refluxed at 45 °C for 12 h. A dark red solution without precipitates was obtained. Removal of the solvent under reduced pressure afforded crude **9** in quantitative yield. For purification, a sublimation apparatus with cooling finger was charged with the crude product and sublimation was carried out at 105 °C overnight to yield 1.41 g (79 %) of **9** as dark red, crystalline solid. **9** : dark red solid, m.p. 154 °C. Sublimation: 110 °C (1 x 10<sup>-1</sup> mbar). **HRMS (EI)** for the molecular ion peak [M]<sup>+</sup>: Found, m/z = 357.2269, calcd. 357.1489. **IR** in ATR mode:  $\nu$  (cm<sup>-1</sup>) = 2966.2 (m), 2926.5 (m), 2867.3 (w), 1732.7 (w), 1684.4 (w), 1633.9 (w), 1572.1 (s), 1464.1 (m), 1437.7 (m), 1387.0 (s), 1364.8 (m), 1333.9 (m), 1262.9 (m), 1209.7 (m), 1185.5 (s), 1091.8 (m), 1027.3 (s), 986.0 (m), 970.5 (m), 951.4 (m), 896.9 (m), 868.4 (m), 815.0 (m), 736.6 (s), 679.9 (m), 610.1 (s), 550.2 (m), 514.3 (m). **EA** calcd. (%): C 60.33, H 7.59, N 15.63; found (%): C 60.21, H 7.31, N 15.82.  $\mu_B$  in C<sub>6</sub>D<sub>6</sub> solution = 4.22 (Evans' method).

#### Bis(N,N-dimethyl(N'-*tert*-butyl)ethane-1-amino-2-amido)cobalt(II) (**10**)

1.44 g (10 mmol) of N,N-dimethyl(N'-*tert*-butyl)ethane-1-amino-2-amine were diluted in 40 ml of Et<sub>2</sub>O and the solution cooled with an ice bath. 5 ml of a 2 M <sup>n</sup>BuLi solution in hexanes were added dropwise under vigorous stirring. The ice bath was removed, stirring continued for 1.5 h and the solution added to a slurry of 0.65 g (5 mmol) CoCl<sub>2</sub> in 60 ml Et<sub>2</sub>O by cannula transfer. The reaction slurry was then refluxed at 45 °C overnight (12 h) and adopted a dark brown to black color. The solvent was removed under reduced pressure, crude **10** extracted with 3 x 20 ml of pentane and filtration carried out using a celite padded frit. As crystallization from hydrocarbons and etheric solvents proved challenging owing to the immense solubility of **10**, the solvent was again removed under reduced pressure and the remaining solid dried in vacuum. Subsequently, vacuum sublimation at 75 °C was carried out and allowed to isolate 0.60 g (35 %) of **10** as black crystalline, needles that were suitable for SC-XRD analysis. **10** : black solid, m.p. 84 °C. Sublimation: 80 °C (1 x 10<sup>-1</sup> mbar). **HRMS (EI)** for the molecular ion peak [M]<sup>+</sup>: Found, m/z = 345.2399, calcd. 345.2428. **IR** in ATR mode:  $\nu$  (cm<sup>-1</sup>) = 2995.9 (m), 2952.3 (s), 2889.6 (m), 2858.1 (m), 2826.6 (m), 2797.0 (m), 2781.1 (m), 2759.7 (m), 2724.3 (m), 2692.8 (w), 2659.3 (w), 1596.4 (m), 1454.3 (s), 1425.2 (m), 1400.6 (w), 1373.5 (m), 1352.8 (m), 1338.6 (s), 1277.4 (m), 1253.5 (s), 1235.0 (s), 1206.7 (s), 1169.7 (m), 1127.0 (m), 1109.6 (s), 1061.8 (m), 1043.2 (m), 1024.7 (m), 1010.5 (s), 994.3 (s), 970.2 (m), 99.6 (m), 912.5 (w), 872.0 (s), 856.9 (m), 787.1 (s), 766.4 (m), 712.9 (w), 682.4 (m), 616.1 (m), 586.5 (m), 570.2

(m), 552.7 (s). **EA** calcd. (%): C 55.59, H 10.63, N 17.63; found (%): C 55.73, H 10.79, N 17.32.  $\mu_B$  in C<sub>6</sub>D<sub>6</sub> solution = 4.85 (Evans' method).

Bis(N,N-dimethyl(N'-trimethylsilyl)ethane-1-amino-2-amido)cobalt(II) (**11**)

Following the procedure described for **10**, 1.60 g (10 mmol) of N'-trimethylsilyl)ethane-1-amino-2-amine were diluted in 40 ml of Et<sub>2</sub>O and lithiated with 5 ml of a 2 M <sup>n</sup>BuLi solution. After stirring for 1.5 h, the solution was transferred to a suspension of 0.65 g (5 mmol) CoCl<sub>2</sub> in 60 ml Et<sub>2</sub>O. The reaction solution turned dark purple within several minutes and was refluxed overnight (12 h) at 45 °C. The solvent was removed under reduced pressure and crude **11** extracted and filtered through a celite padded frit with 3 x 20 ml of pentane. Subsequent solvent removal yielded a purple solid that was purified by vacuum sublimation at 80 °C. 1.59 g (84 %) of needle-shaped **11** were obtained. **11** : purple solid, m.p. 90 °C. Sublimation: 85 °C (1 x 10<sup>-1</sup> mbar). **HRMS (EI)** for the molecular ion peak [M]<sup>+</sup>: Found, m/z = 377.1858, calcd. 377.1967. **IR** in ATR mode:  $\nu$  (cm<sup>-1</sup>) = 2997.4 (w), 2942.8 (m), 2889.9 (m), 2864.7 (m), 2832.5 (m), 2788.9 (m), 2709.0 (w), 2660.8 (w), 1474.2 (m), 1453.5 (m), 1428.3 (w), 1402.7 (w), 1361.4 (w), 1339.6 (m), 1272.8 (m), 1248.9 (m), 1233.1 (s), 1171.6 (m), 1157.3 (m), 1093.7 (s), 1057.0 (m), 1028.3 (m), 1015.4 (m), 964.1 (s), 939.0 (m), 866.5 (m), 843.0 (s), 818.9 (s), 772.0 (s), 738.7 (s), 671.4 (m), 662.3 (s), 618.5 (m), 562.6 (m). **EA** calcd. (%): C 44.41, H 10.14, N 14.84; found (%): C 44.53, H 10.14, N 14.99.  $\mu_B$  in C<sub>6</sub>D<sub>6</sub> solution = 4.64 (Evans' method).

Bis(bis(4-methyl-N-(trimethylsilyl)pyridine-2-amido)cobalt(II)) (**12**)

4-methyl-N-(trimethylsilyl)pyridine-2-amine (1.80 g, 10 mmol) were diluted in 50 ml of Et<sub>2</sub>O and lithiated with 5 ml of a 2 M <sup>n</sup>BuLi solution. After stirring for 1 h at room temperature, the resulting opaque solution was added to a suspension of 0.65 g (5 mmol) CoCl<sub>2</sub>. Upon refluxing at 45 °C under vigorous stirring overnight, a dark green solution with precipitated LiCl in it was obtained. The solvent was removed under reduced pressure and crude **12** dissolved in 80 ml pentane. Subsequent to filtration through a celite padded frit, the pentane was removed under reduced pressure until the formation of green crystallites was observed. At this point the solution was warmed to room temperature again and stored at -30 °C overnight to yield a first batch of a dark green crystalline solid. The mother liquor was filtered off and the solid dried in vacuum. A second batch of the product was obtained from the concentrated liquor. In total 1.59 g (76 %) of **12** were afforded by this procedure. **12** : dark green solid, m.p. 85 °C (decomposition). Sublimation: not successful. **HRMS (EI)** for the molecular ion peak [M]<sup>+</sup>: Calcd. 834.2682 but not detected; neither was the [M]<sup>+</sup> peak for a monomeric species (417.1341) detected. **IR** in ATR mode:  $\nu$  (cm<sup>-1</sup>) = 2950.2 (w), 2895.3 (w), 1601.0 (m), 1548.5



(w), 1531.9 (m), 1471.3 (m), 1435.4 (m), 1425.1 (m), 1404.6 (m), 1321.6 (m), 1321.6 (m), 1294.7 (m), 1286.1 (m), 1273.5 (m), 1257.6 (m), 1243.2 (m), 1176.4 (m), 1163.3 (m), 1122.8 (m), 1051.8 (w), 1024.3 (m), 996.0 (m), 965.7 (m), 954.7 (m), 877.2 (s), 854.8 (m), 830.2 (s, br.), 807.0 (s), 784.7 (s), 764.3 (m), 746.3 (m), 721.8 (m), 679.1 (m), 622.7 (m), 602.3 (m), 591.6 (m), 572.0 (m), 548.9 (m), 533.0 (m). **EA** calcd. (%): C 51.78, H 7.24, N 13.42; found (%): C 51.22, H 7.09, N 13.59.  $\mu_B$  in C<sub>6</sub>D<sub>6</sub> solution = 5.21 (Evans' method).

### X-ray crystallography:

Owing to the extreme air and moisture sensitivity of the compounds (especially applicable to **4** and **10** which decompose instantaneously), crystals suitable for single crystal X-ray diffraction were admixed in perfluoroalkylether oil in a glovebox and transferred to an external microscope where suitable crystals were rapidly chosen and mounted to the diffractometer (Bruker XtaLAB Synergy, Dualflex, HyPix). The crystals were kept at 100.00 K during data collection. Using Olex2,<sup>[41]</sup> the structure was solved with the SHELXT<sup>[42]</sup> structure solution program using Intrinsic Phasing and refined with the SHELXL<sup>[42]</sup> refinement package using Least Squares minimization. Table 2 summarizes relevant crystallographic data and data acquisition parameters for **2** - **4**, **6** - **8** and **10** - **12**. In this study, the Diamond software was used for molecular structure visualization.<sup>[43]</sup> In addition, the Mercury 2020 software was utilized for short contact and solid state structure packing analysis.<sup>[44]</sup>

- [1] A. Werner, *Z. Anorg. Chem.* 1893, **3**, 267.
- [2] A. Werner, *Ber. Dtsch. Chem. Ges.* 1911, **44**, 1887.
- [3] A. Devi, *Coordination Chemistry Reviews* 2013, **257**, 3332.
- [4] S. E. Koponen, P. G. Gordon, S. T. Barry, *Polyhedron* 2016, **108**, 59.
- [5] a) D. Zanders, G. Bačić, D. Leckie, O. Odegbesan, J. Rawson, J. D. Masuda, A. Devi, S. T. Barry, *Angewandte Chemie (International ed. in English)* 2020, **59**, 14138; b) D. Zanders, J. Liu, J. Obenlünenschloß, C. Bock, D. Rogalla, L. Mai, M. Nolan, S. T. Barry, A. Devi, *Chem. Mater.* 2021.
- [6] a) H. Kim, H.-B.-R. Lee, W.-J. Maeng, *Thin Solid Films* 2009, **517**, 2563; b) M. Leskelä, M. Mattinen, M. Ritala, *Journal of Vacuum Science & Technology B* 2019, **37**, 30801; c) P. Poodt, D. C. Cameron, E. Dickey, S. M. George, V. Kuznetsov, G. N. Parsons, F. Roozeboom, G. Sundaram, A. Vermeer, *Journal of Vacuum Science & Technology A: Vacuum, Surfaces, and Films* 2012, **30**, 10802; d) D. J. Emslie, P. Chadha, J. S. Price, *Coordination Chemistry Reviews* 2013, **257**, 3282; e) F. Zaera, *Coordination Chemistry Reviews* 2013, **257**, 3177.
- [7] S. M. George, *Chemical reviews* 2010, **110**, 111.
- [8] a) Z. Guo, X. Wang, *Angewandte Chemie (International ed. in English)* 2018, **57**, 5898; b) H. Kim, H.-B.-R. Lee, W.-H. Kim, J. W. Lee, J. Kim, I. Hwang, *J. Korean Phy. Soc.* 2010, **56**, 104.
- [9] a) J. P. Klesko, M. M. Kerrigan, C. H. Winter, *Chem. Mater.* 2016, **28**, 700; b) M. M. Kerrigan, J. P. Klesko, C. H. Winter, *Chem. Mater.* 2017, **29**, 7458.
- [10] T. Iivonen, M. Kaipio, T. Hatanpää, K. Mizohata, K. Meinander, J. Räisänen, J. Kim, M. Ritala, M. Leskelä, *Journal of Vacuum Science & Technology A* 2019, **37**, 10908.
- [11] A. M. Bryan, G. J. Long, F. Grandjean, P. P. Power, *Inorganic chemistry* 2013, **52**, 12152.
- [12] B. M. Day, K. Pal, T. Pugh, J. Tuck, R. A. Layfield, *Inorganic chemistry* 2014, **53**, 10578.

- [13] A. Eichhöfer, Y. Lan, V. Mereacre, T. Bodenstein, F. Weigend, *Inorganic chemistry* 2014, 53, 1962.
- [14] S. N. König, C. Schädle, C. Maichle-Mössmer, R. Anwander, *Inorganic chemistry* 2014, 53, 4585.
- [15] C.-Y. Lin, J. C. Fetting, P. P. Power, *Inorganic chemistry* 2017, 56, 9892.
- [16] A. Massard, P. Braunstein, A. A. Danopoulos, S. Choua, P. Rabu, *Organometallics* 2014, 34, 2429.
- [17] I. Müller, C. Schneider, C. Pietzonka, F. Kraus, C. G. Werncke, *Inorganics* 2019, 7, 117.
- [18] T. Chen, W. Hunks, P. S. Chen, G. T. Stauf, T. M. Cameron, C. Xu, A. G. DiPasquale, A. L. Rheingold, *Eur. J. Inorg. Chem.* 2009, 2009, 2047.
- [19] H. Drevs, A. Schmeißer, H. Hartung, U. Baumeister, *Chem. Ber.* 1996, 129, 853.
- [20] G. Glatz, S. Demeshko, G. Motz, R. Kempe, *Eur. J. Inorg. Chem.* 2009, 2009, 1385.
- [21] C. H. Wei, *Inorg. Chem.* 1972, 11, 1100.
- [22] R. H. Holm, A. Chakravorty, L. J. Theriot, *Inorg. Chem.* 1966, 5, 625.
- [23] D. F. Evans, *J. Chem. Soc.* 1959, 2003.
- [24] S. N. König, D. Schneider, C. Maichle-Mössmer, B. M. Day, R. A. Layfield, R. Anwander, *Eur. J. Inorg. Chem.* 2014, 2014, 4302.
- [25] M. G. Gardiner, C. L. Raston, B. W. Skelton, A. H. White, *Inorganic chemistry* 1997, 36, 2795.
- [26] a) G.-H. Chen, W.-J. Leu, J.-H. Guh, C.-H. Lin, J.-H. Huang, *Journal of Organometallic Chemistry* 2018, 868, 122; b) Z. Feng, Z. Huang, S. Wang, Y. Wei, S. Zhou, X. Zhu, *Dalton transactions (Cambridge, England : 2003)* 2019, 48, 11094; c) J.-H. Huang, H.-J. Chen, C.-C. Hsieh, G.-H. Lee, S.-M. Peng, *Inorganica Chimica Acta* 2001, 321, 142; d) R. Inoue, Y. Morisaki, *Eur. J. Inorg. Chem.* 2020, 2020, 3959; e) J. D. Parish, M. W. Snook, A. L. Johnson, G. Kociok-Köhn, *Dalton transactions (Cambridge, England : 2003)* 2018, 47, 7721.
- [27] K. J. Blakeney, C. H. Winter, *Chem. Mater.* 2018, 30, 1844.
- [28] J. M. Bakker, G. B. Deacon, P. C. Junk, G. J. Moxey, D. R. Turner, *Z. anorg. allg. Chem.* 2007, 633, 251.
- [29] M. Lappert, *Metal amide chemistry*, Wiley, Chichester, 2009.
- [30] R. Kempe, P. Arndt, *Inorganic chemistry* 1996, 35, 2644.
- [31] M. C. Barral, E. Delgado, E. Gutiérrez-Puebla, R. Jimenez-Aparicio, A. Monge, C. Del Pino, A. Santos, *Inorganica Chimica Acta* 1983, 74, 101.
- [32] L. Yang, D. R. Powell, R. P. Houser, *Dalton transactions (Cambridge, England : 2003)* 2007, 955.
- [33] A. Okuniewski, D. Rosiak, J. Chojnacki, B. Becker, *Polyhedron* 2015, 90, 47.
- [34] G. Glatz, R. Kempe, *Zeitschrift für Kristallographie - New Crystal Structures* 2008, 223, 313.
- [35] A. W. Addison, T. N. Rao, J. Reedijk, J. van Rijn, G. C. Verschoor, *J. Chem. Soc., Dalton Trans.* 1984, 1349.
- [36] A. E. Kaloyeros, Y. Pan, J. Goff, B. Arkles, *ECS J. Solid State Sci. Technol.* 2019, 8, P119-P152.
- [37] G. Bačić, D. Zanders, B. Mallick, A. Devi, S. T. Barry, *Inorganic chemistry* 2018, 57, 8218.
- [38] J. Raynaud, J. Y. Wu, T. Ritter, *Angewandte Chemie (International ed. in English)* 2012, 51, 11805.
- [39] W. Herz, K. Dittmer, S. J. Cristol, *J. Am. Chem. Soc.* 1947, 69, 1698.
- [40] V. Grushin, W. Marshall, *Advanced Synthesis & Catalysis* 2004, 346, 1457.
- [41] O. V. Dolomanov, L. J. Bourhis, R. J. Gildea, J. A. K. Howard, H. Puschmann, *Journal of applied crystallography* 2009, 42, 339.
- [42] G. M. Sheldrick, *Acta crystallographica. Section A, Foundations and advances* 2015, 71, 3.
- [43] Crystal Impact - Dr. H. Putz & Dr. K. Brandenburg GbR, *Diamond - Crystal and Molecular Structure Visualization*, Kreuzherrenstr. 102, 53227 Bonn, Germany.
- [44] C. F. Macrae, I. Sovago, S. J. Cottrell, P. T. A. Galek, P. McCabe, E. Pidcock, M. Platings, G. P. Shields, J. S. Stevens, M. Towler et al., *Journal of applied crystallography* 2020, 53, 226.

Supporting Information for:

# Co(II) Amide, Pyrrolate and Amidopyridine Complexes: Assessment of their Manifold Structural Chemistry and Thermal Properties

D. Zanders,<sup>[a,b]</sup> N. Boysen,<sup>[a]†</sup> M. A. Land,<sup>[b]†</sup> J. Obenlünenschloß,<sup>[a]</sup> J. D. Masuda,<sup>[c]</sup> B.  
Mallick,<sup>[d]</sup> S. T. Barry,<sup>[b]</sup> A. Devi<sup>[a]</sup> \*

[a] Inorganic Materials Chemistry, Ruhr University Bochum, Universitätsstraße 150, Bochum, 44801 Germany

[b] Department of Chemistry, Carleton University, 1125 Colonel By Drive, Ottawa, Ontario, K1S 5B6 Canada

[c] Department of Chemistry, Saint Mary's University, 923 Robie Street, Halifax, Nova Scotia, B3H 3C3 Canada

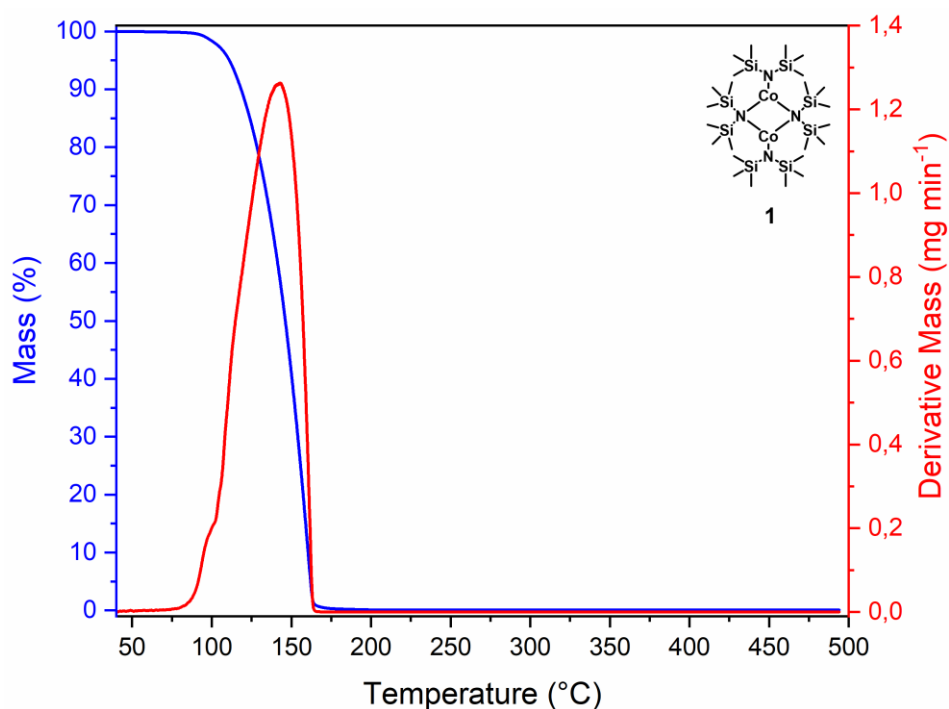
[d] Chair of Inorganic Chemistry II, Ruhr University Bochum, Universitätsstraße 150, Bochum, 44801 Germany

## Table of Contents

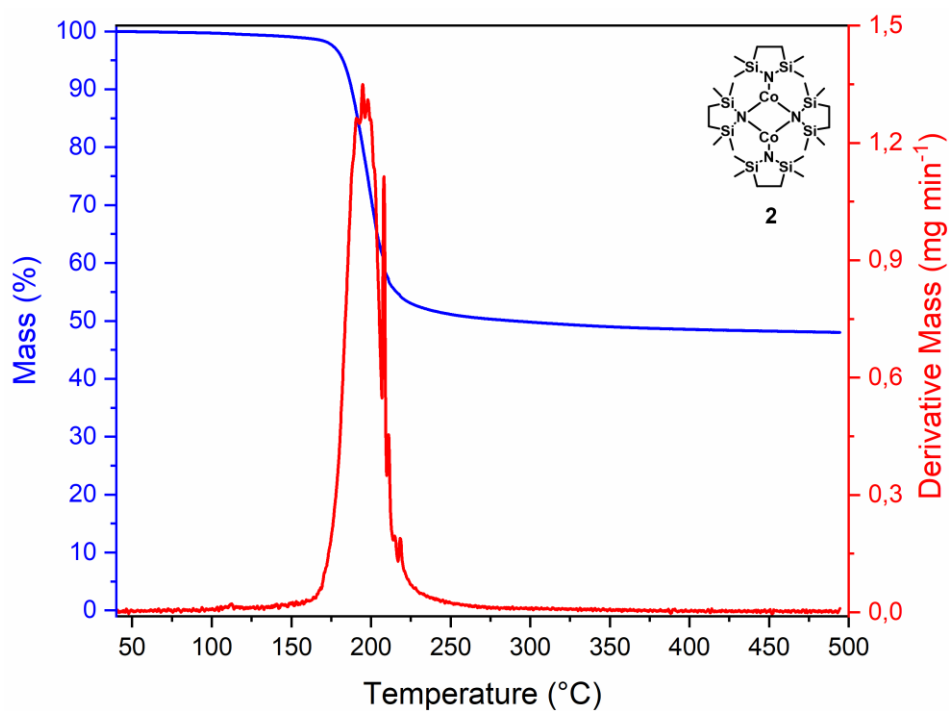
### Page

1. Thermogravimetric Analysis (TGA) .....	2
2. Infrared (IR) Spectroscopy .....	8
3. Additional Crystallographic Details and Images .....	14
4. References .....	17

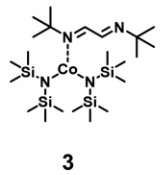
## 1. Thermogravimetric Analysis (TGA)



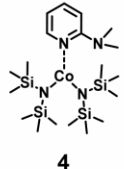
**Figure S 1:** Thermogravimetric analysis of [Co(TMSA)<sub>2</sub>]<sub>2</sub> **1** with a heating rate of 10 °C min<sup>-1</sup>. The loaded mass was 10.2 mg and the residual mass was 0.1 %.




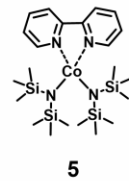
**Figure S 2:** Thermogravimetric analysis of [Co(TMADS)<sub>2</sub>]<sub>2</sub> **2** with a heating rate of 10 °C min<sup>-1</sup>. The loaded mass was 10.2 mg and the residual mass was 48.0 %.



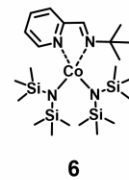
**4**



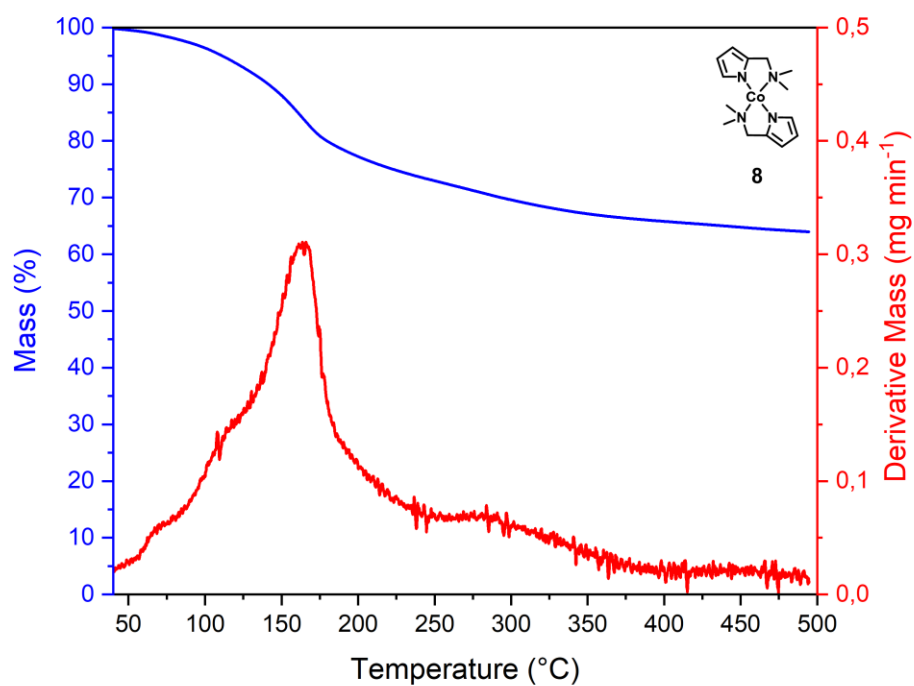
**Figure S 4:** Thermogravimetric analysis of [Co(TMSA)<sub>2</sub>(DMAPY)] **4** with a heating rate of 10 °C min<sup>-1</sup>. The loaded mass was 9.8 mg and the residual mass was 17.9 %.



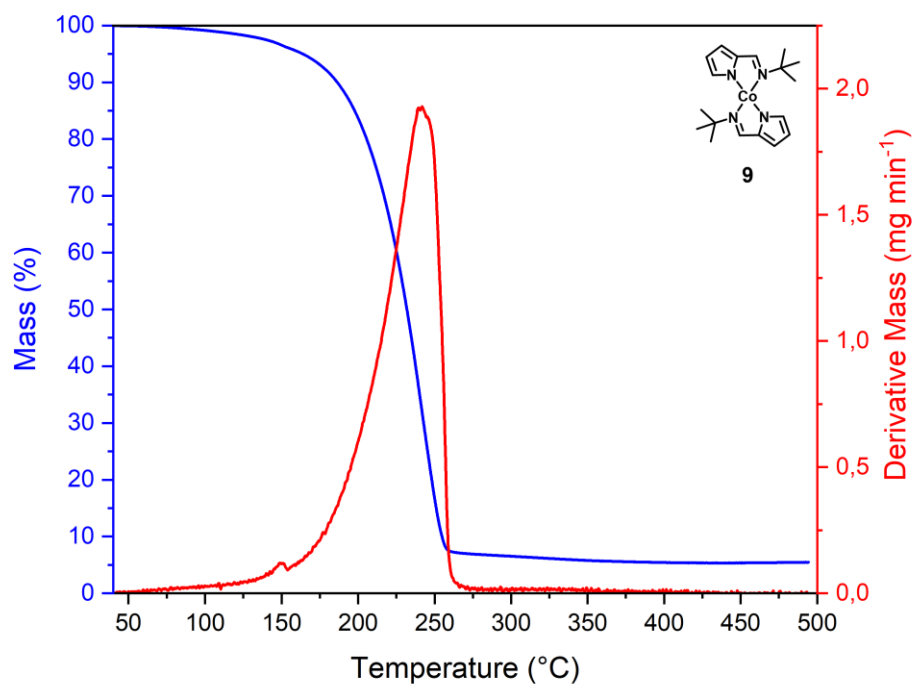
**6**



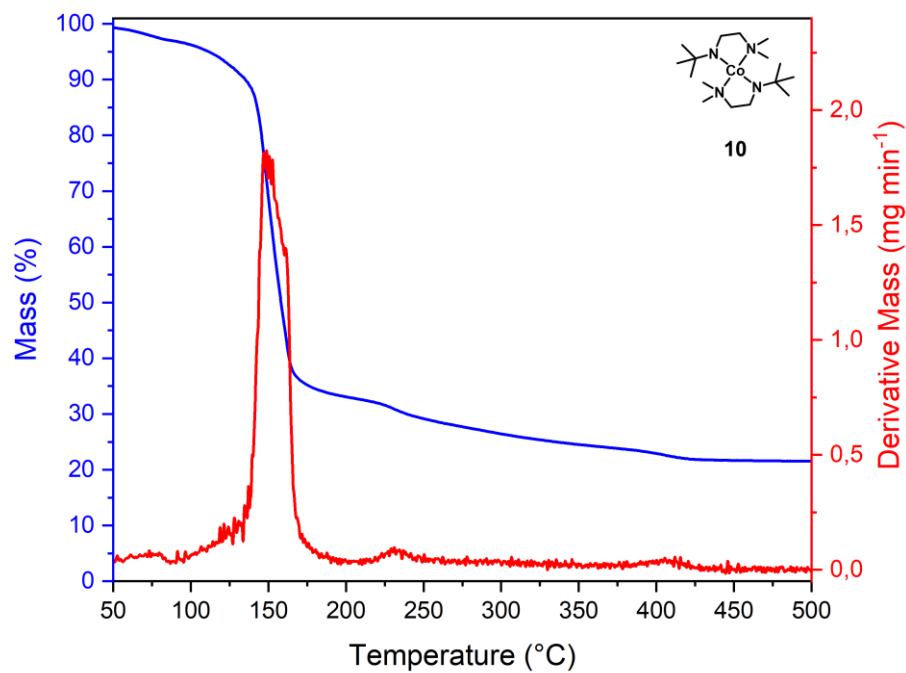
**Figure S 6:** Thermogravimetric analysis of [Co(TMSA)<sub>2</sub>(IMPY)] **6** with a heating rate of 10 °C min<sup>-1</sup>. The loaded mass was 10.7 mg and the residual mass was 26.7 %.



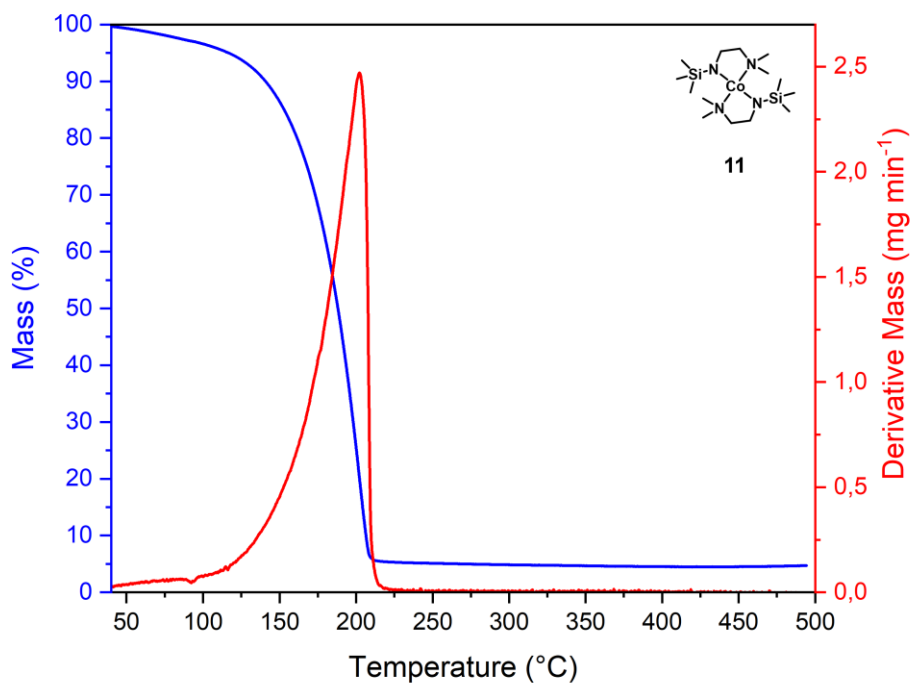
**Figure S 7:** Thermogravimetric analysis of  $[\text{Co}(\text{AMPR})_2]$  **8** with a heating rate of  $10\text{ }^\circ\text{C min}^{-1}$ . The loaded mass was 10.1 mg and the residual mass was 64.1 %.



**Figure S 8:** Thermogravimetric analysis of  $[\text{Co}(\text{IMPR})_2]$  **9** with a heating rate of  $10\text{ }^\circ\text{C min}^{-1}$ . The loaded mass was 10.1 mg and the residual mass was 5.5 %.

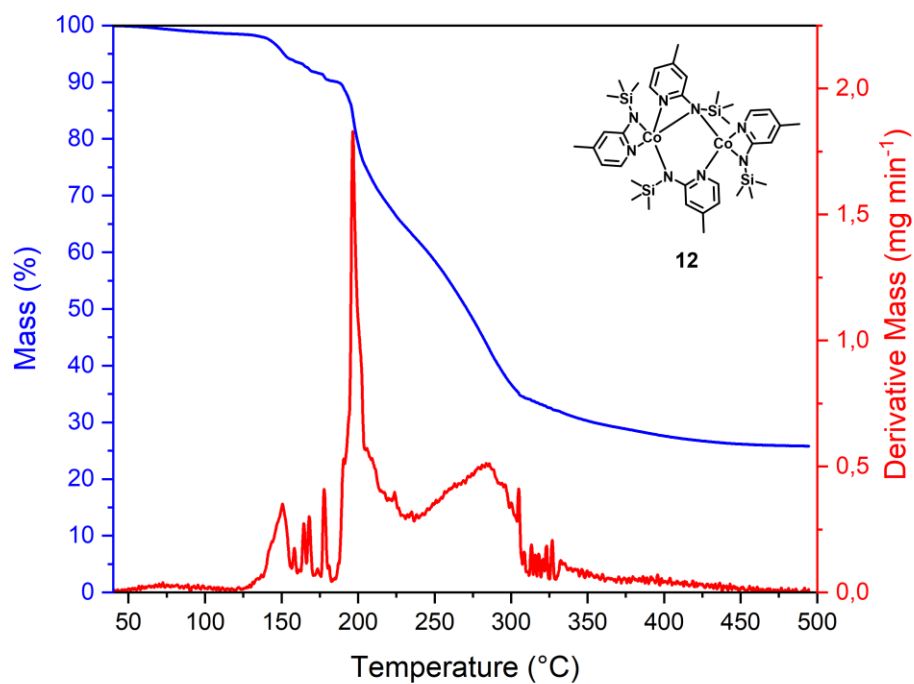


**Figure S 9:** Thermogravimetric analysis of  $[\text{Co}(\text{TBUAEDMA})_2]$  **10** with a heating rate of  $10\text{ }^\circ\text{C min}^{-1}$ . The loaded mass was 11.0 mg and the residual mass was 21.4 %.



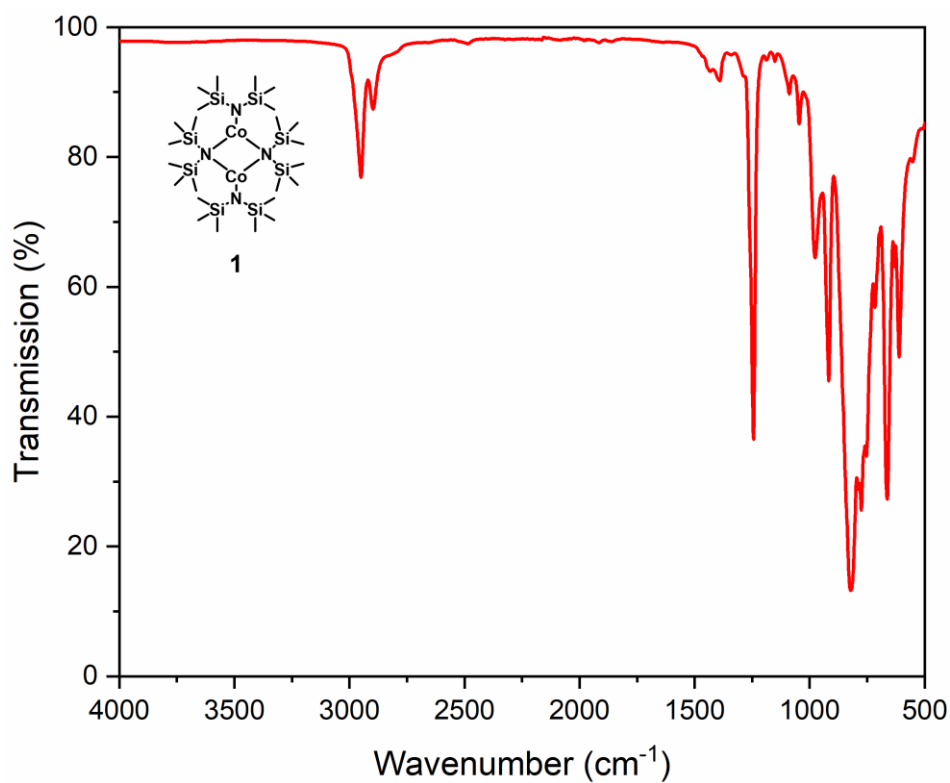
**Figure S 10:** Thermogravimetric analysis of  $[\text{Co}(\text{TMSAEDMA})_2]$  **11** with a heating rate of  $10\text{ }^\circ\text{C min}^{-1}$ . The loaded mass was 10.0 mg and the residual mass was 4.7 %.



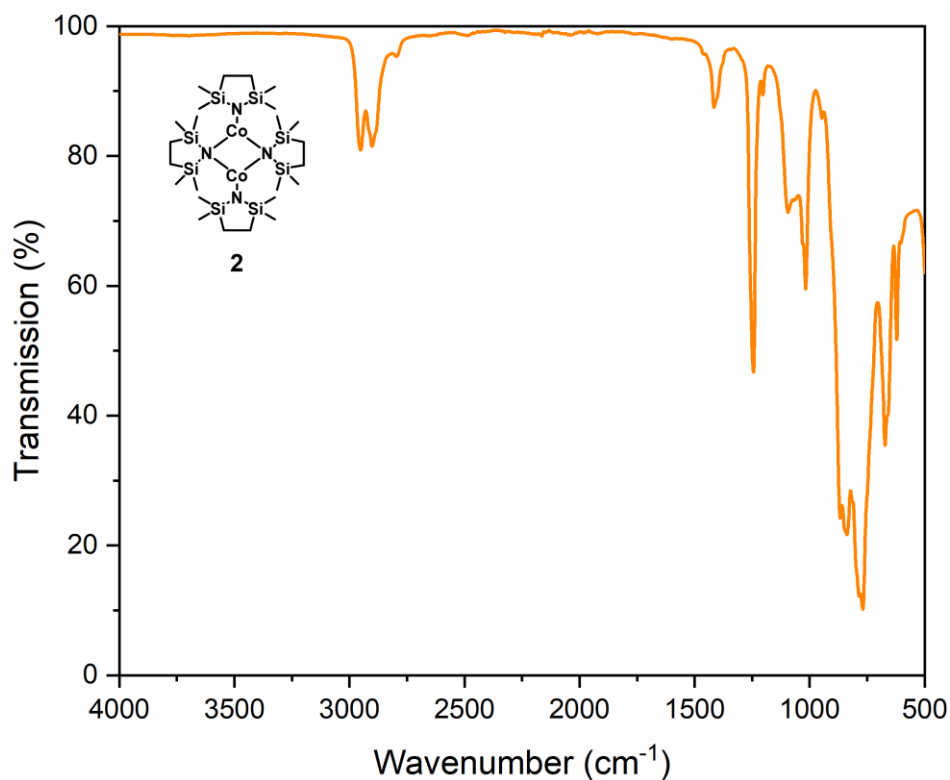


**Figure S 11:** Thermogravimetric analysis of  $[\text{Co}(\text{TMSMAPY})_2]_2$  **12** with a heating rate of  $10\text{ }^\circ\text{C min}^{-1}$ . The loaded mass was 10.1 mg and the residual mass was 25.8 %.

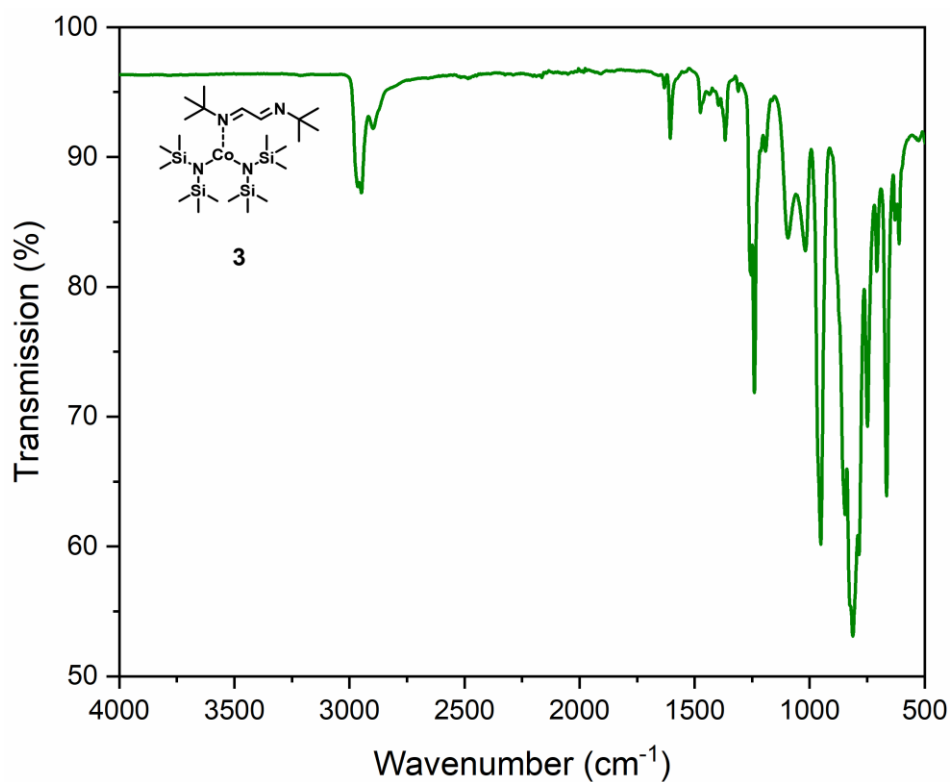
## 2. Infrared (IR) Spectroscopy



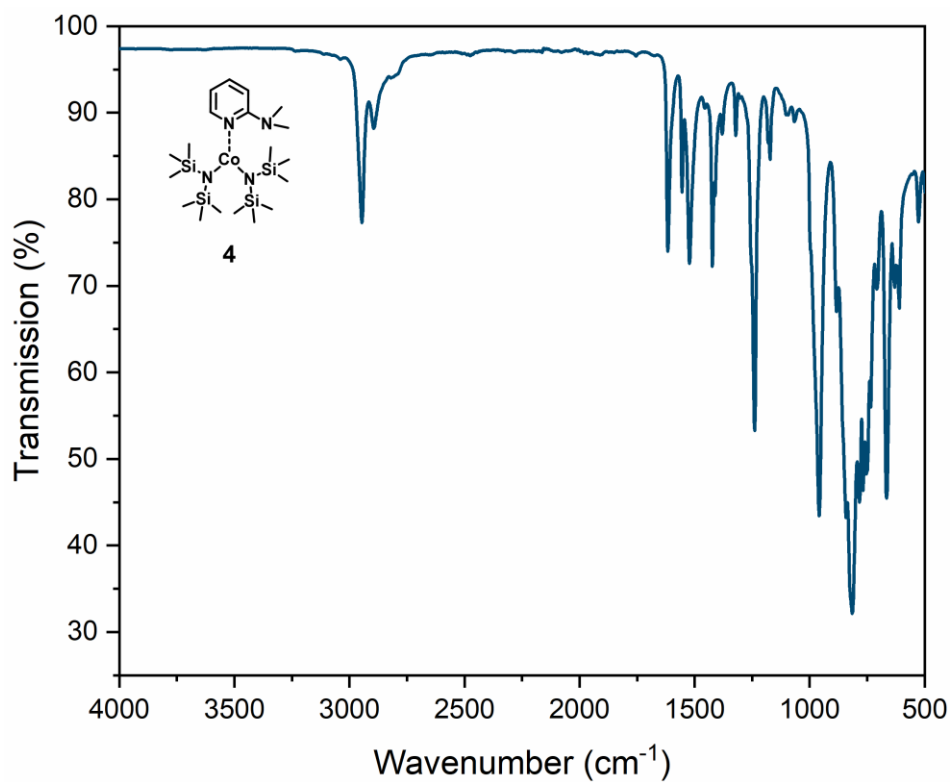
**Figure S 12:** Infrared spectroscopy spectrum of [Co(TMSA)<sub>2</sub>]<sub>2</sub> **1** recorded with an ATR unit.



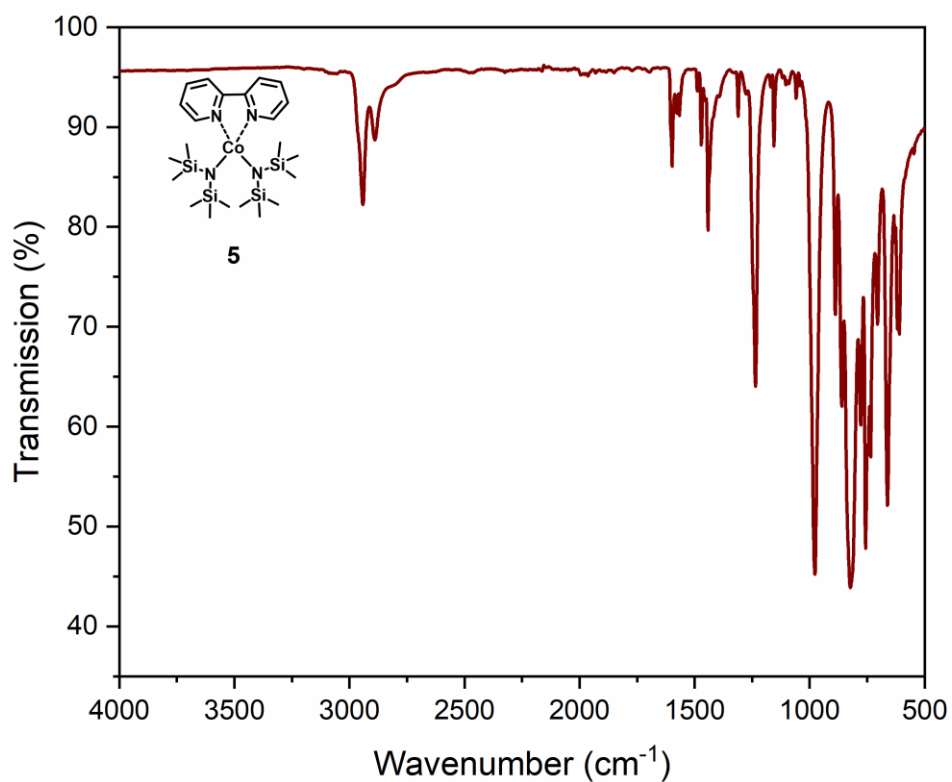
**Figure S 13:** Infrared spectroscopy spectrum of [Co(TMADS)<sub>2</sub>]<sub>2</sub> **2** recorded with an ATR unit.



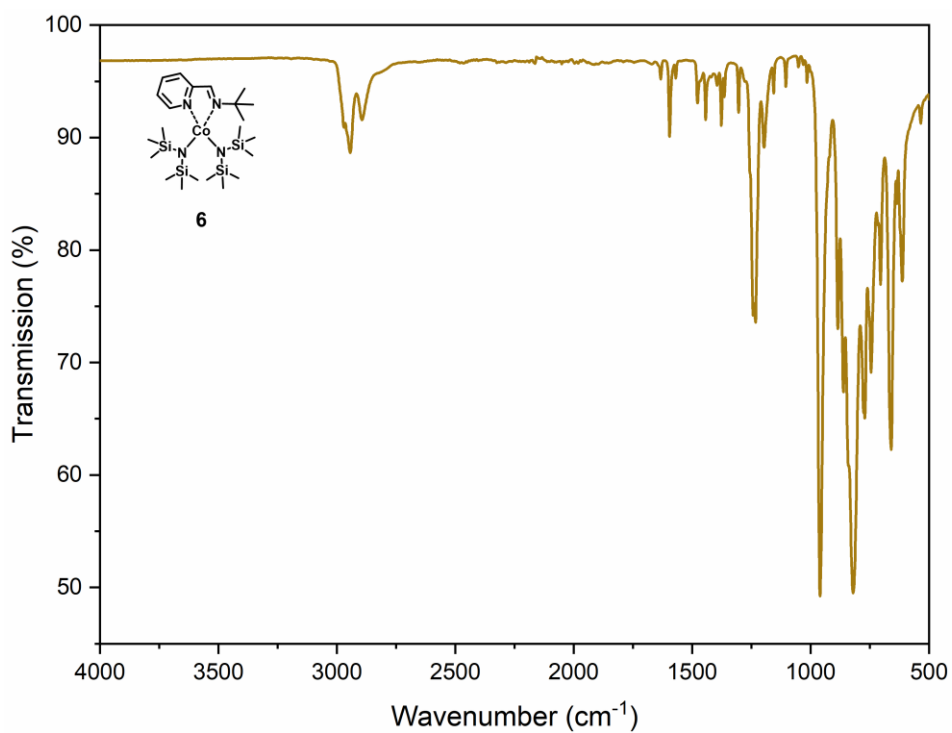
**Figure S 14:** Infrared spectroscopy spectrum of  $[\text{Co}(\text{TMSA})_2(\text{DAD})]$  **3** recorded with an ATR unit.



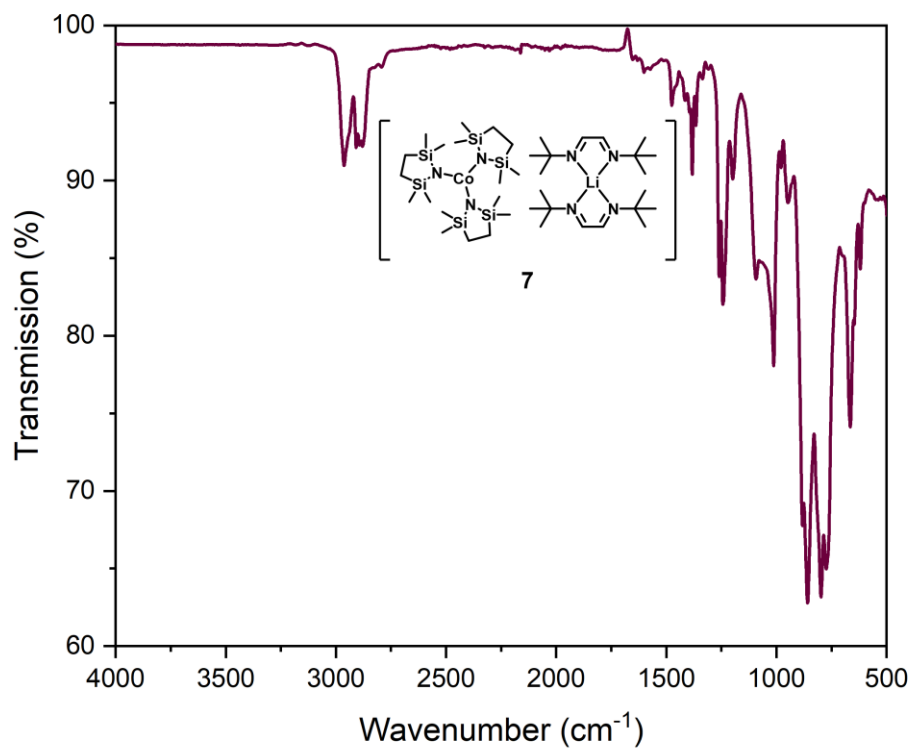
**Figure S 15:** Infrared spectroscopy spectrum of  $[\text{Co}(\text{TMSA})_2(\text{DMAPY})]$  **4** recorded with an ATR unit.



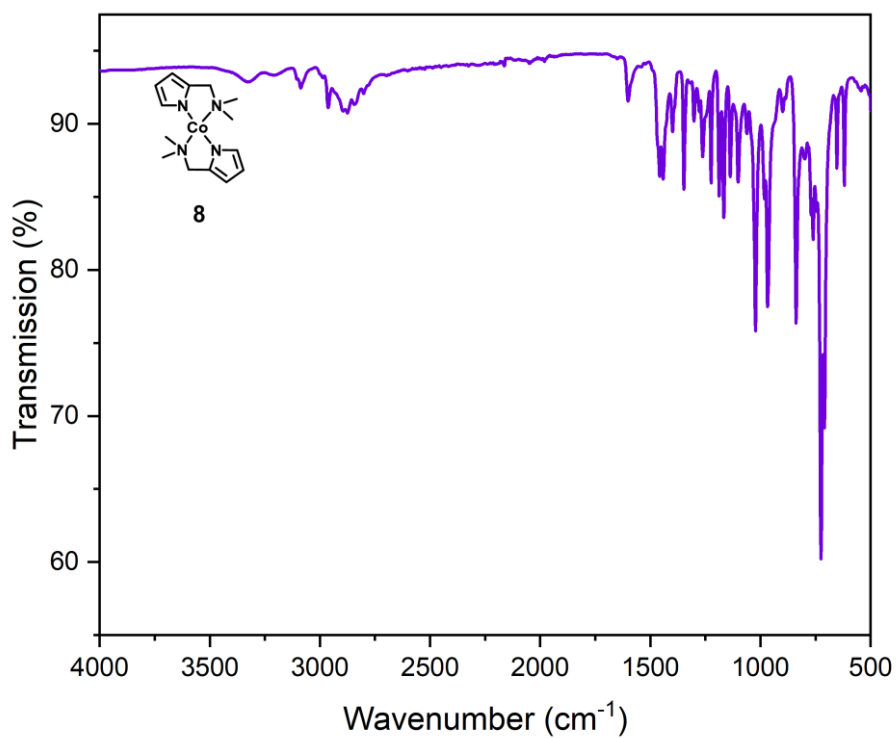
**Figure S 16:** Infrared spectroscopy spectrum of [Co(TMSA)<sub>2</sub>(BIPY)] **5** recorded with an ATR unit.



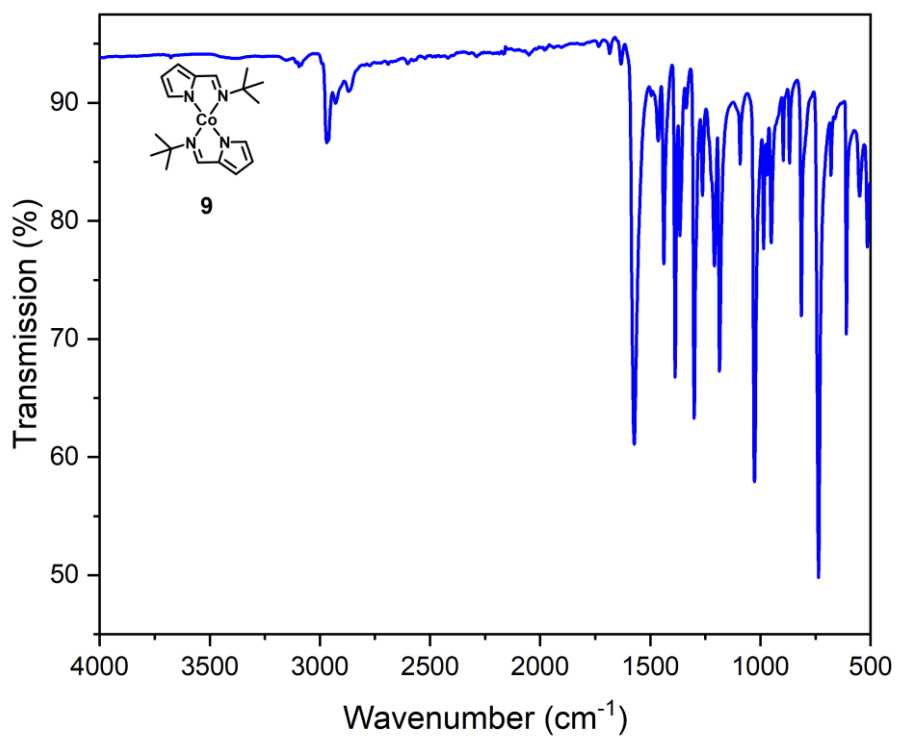
**Figure S 17:** Infrared spectroscopy spectrum of [Co(TMSA)<sub>2</sub>(IMPY)] **6** recorded with an ATR unit.



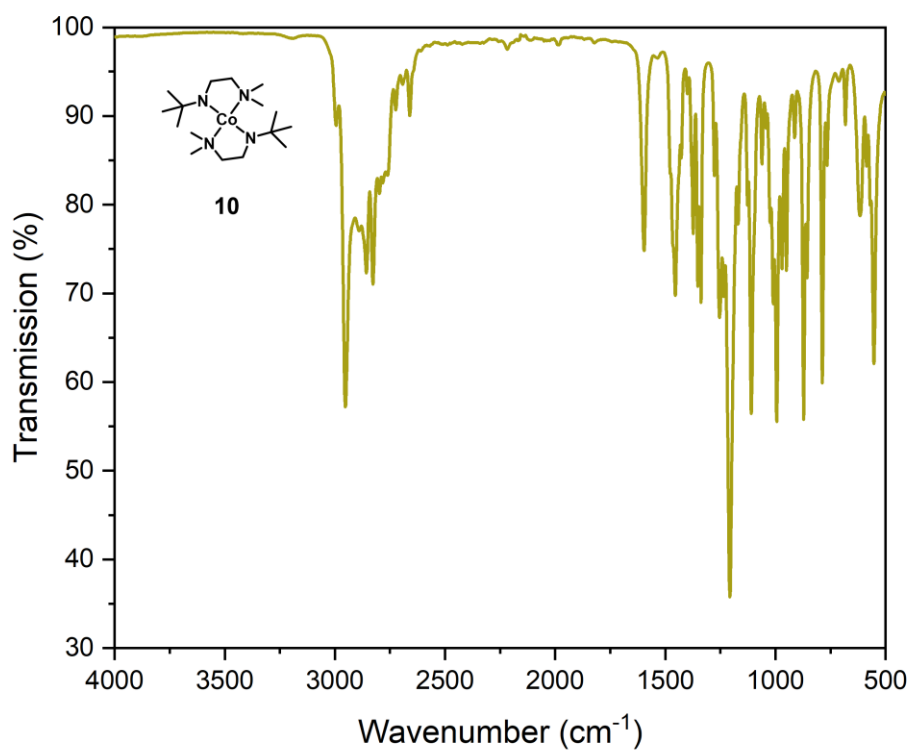
**Figure S 18:** Infrared spectroscopy spectrum of  $[\text{Co}(\text{TMADS})_3\text{Li}(\text{DAD})_2]$  **7** recorded with an ATR unit.



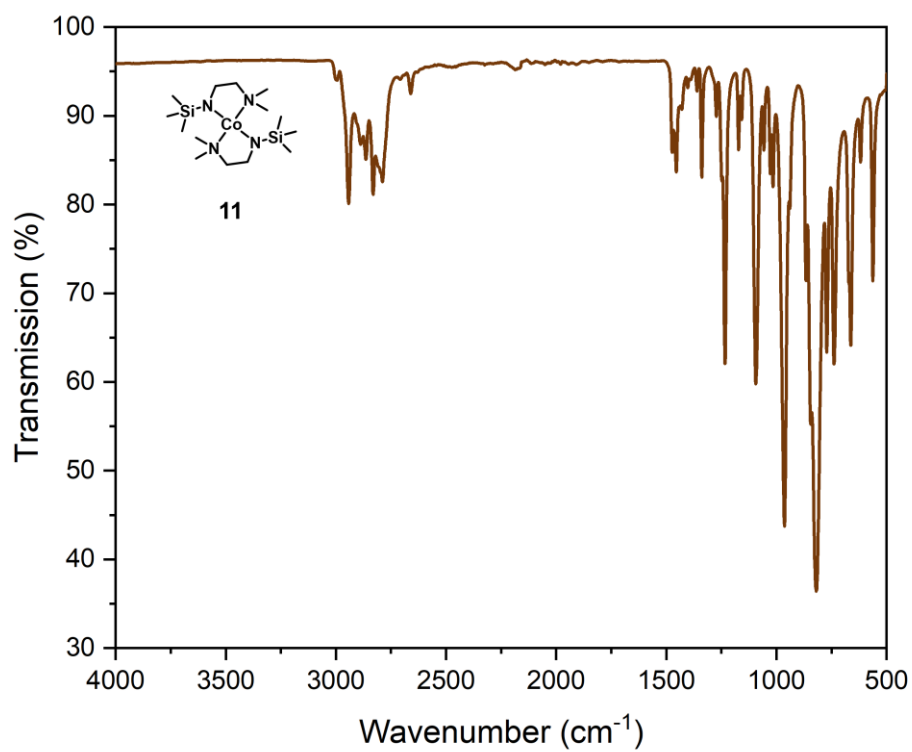
**Figure S 19:** Infrared spectroscopy spectrum of  $[\text{Co}(\text{AMPR})_2]$  **8** recorded with an ATR unit.



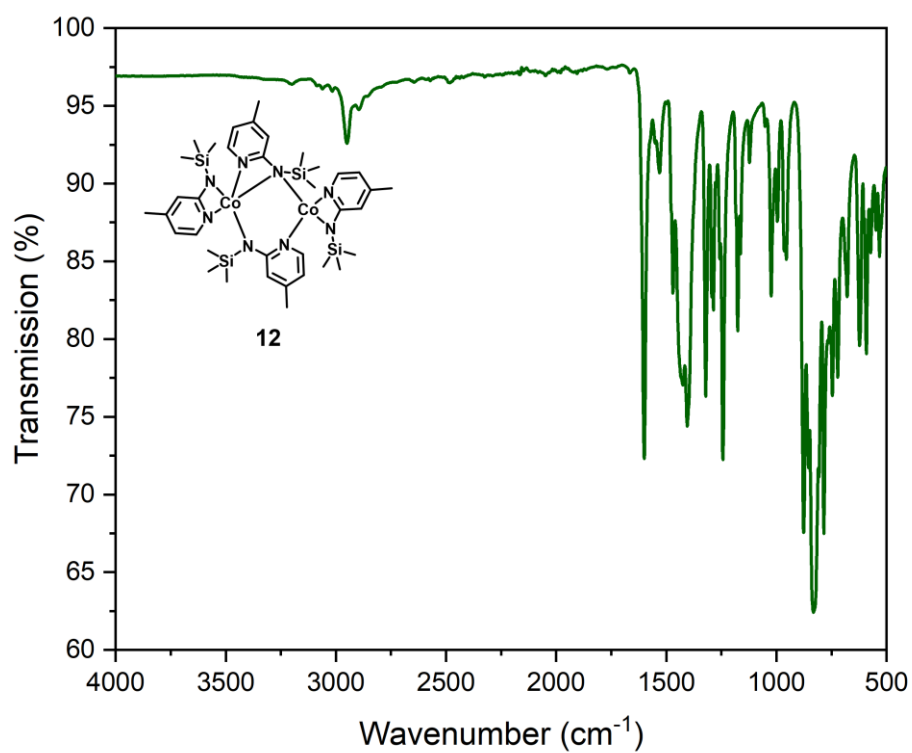
**Figure S 20:** Infrared spectroscopy spectrum of [Co(IMPR)<sub>2</sub>] **9** recorded with an ATR unit.



**Figure S 21:** Infrared spectroscopy spectrum of [Co(TBUAEDMA)<sub>2</sub>] **10** recorded with an ATR unit.



**Figure S 22:** Infrared spectroscopy spectrum of [Co(TMSAEDMA)<sub>2</sub>] **11** recorded with an ATR unit.



**Figure S 23:** Infrared spectroscopy spectrum of [Co(TSMAPY)<sub>2</sub>] **12** recorded with an ATR unit.

### 3. Additional Crystallographic Details and Images

Specific details on individual disorders and structure refinements:

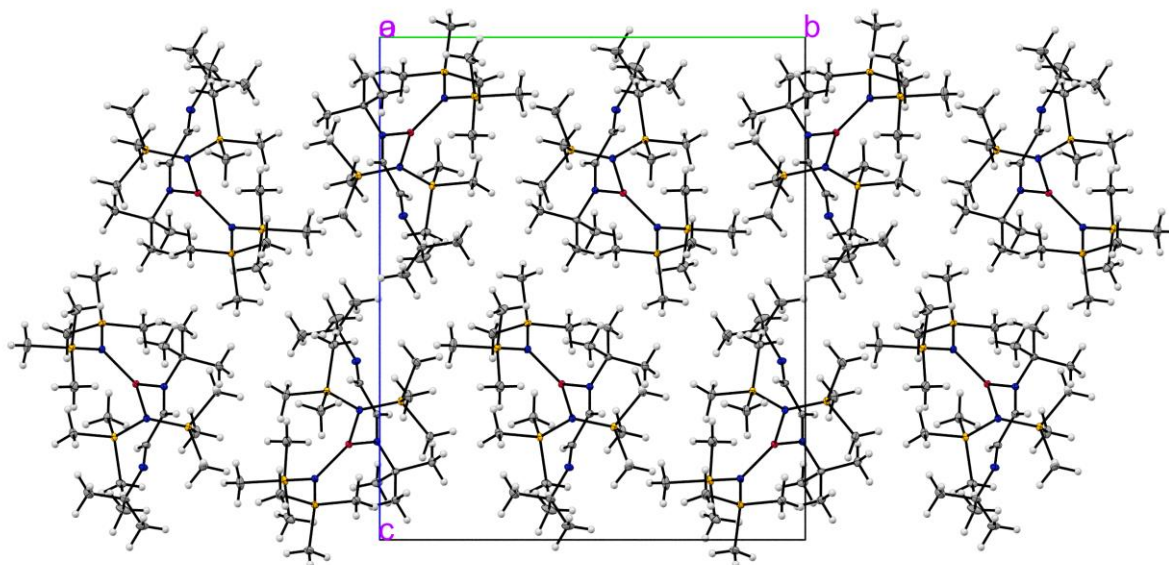
**Compound 4:** For this compound, the DMAPY ligand was found to possess two strongly intercontorted positions. This double-position could not be described by a space group with higher symmetry, however and was thus identified as significant distortion. Besides, both TMSA ligands were found to be systematically disordered whereby the  $\text{Si}(\text{CH}_3)_3$  groups exhibited rotatory distortions, and the nitrogen atoms positional distortions. Satisfying structure solution was only achieved by assigning two positions to the central  $\text{Co}(\text{II})$  ion as well and by describing the entire molecule by two different parts differentiating the distortions.

**Compound 10:** For this compound, all samples subjected to single crystal XRD analysis yielded data sets in which the  $\text{Co}(\text{TBUAEDMA})_2$  molecules were strongly distorted. More precisely, the central  $\text{Co}(\text{II})$  ion was found to be surrounded by each of the TBUAEDMA ligands in two different ways. TBUAEDMA consists of a monoanionic  $^t\text{BuN}$  amido moiety that is connected via a  $\text{CH}_2\text{--CH}_2$  backbone chain to a neutral  $\text{N}(\text{CH}_3)_2$  amino moiety. Averaged over a large number of molecules, one fraction of the covalently bonding  $^t\text{BuN}$  amide is found at one position while the other fraction is found at a clearly different one. The same is true for the  $\text{N}(\text{CH}_3)_2$  amino moieties. As a result, each of the ligands can fold around the central ion in two ways. The bridging  $\text{CH}_2\text{--CH}_2$  backbone adopts different positions as well. A satisfying structure solution was achieved by describing this double position by two parts for each ligand.

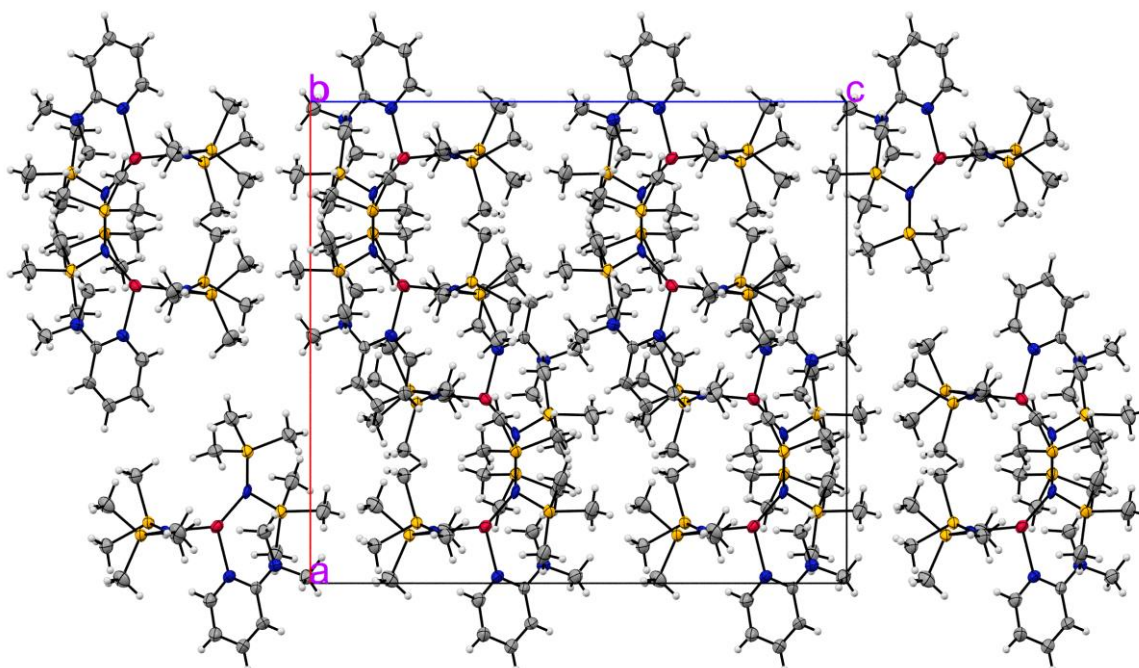
**Compound 11:** The main disorder found in this compound is strongly related to the one found for compound **10**. It needs to be highlighted again, that several samples were subjected to single crystal XRD analysis and that for all of them the same type of disorder was found. In analogy to the TBUAEDMA ligand, the TMSAEDMA ligand can fold itself around the  $\text{Co}(\text{II})$  central ion in two different ways that need to be described by two parts to obtain a satisfying structure solution. The disorder was found for eight of thirteen molecules in the unit cell.

**Compound 12:** In  $[\text{Co}(\text{TMSMAPY})_2]_2$ , a single  $\text{Si}(\text{CH}_3)_3$  group of one of the TMSMAPY ligands exhibits a rotatory disorder that needed to be modeled to obtain a satisfying structure solution.

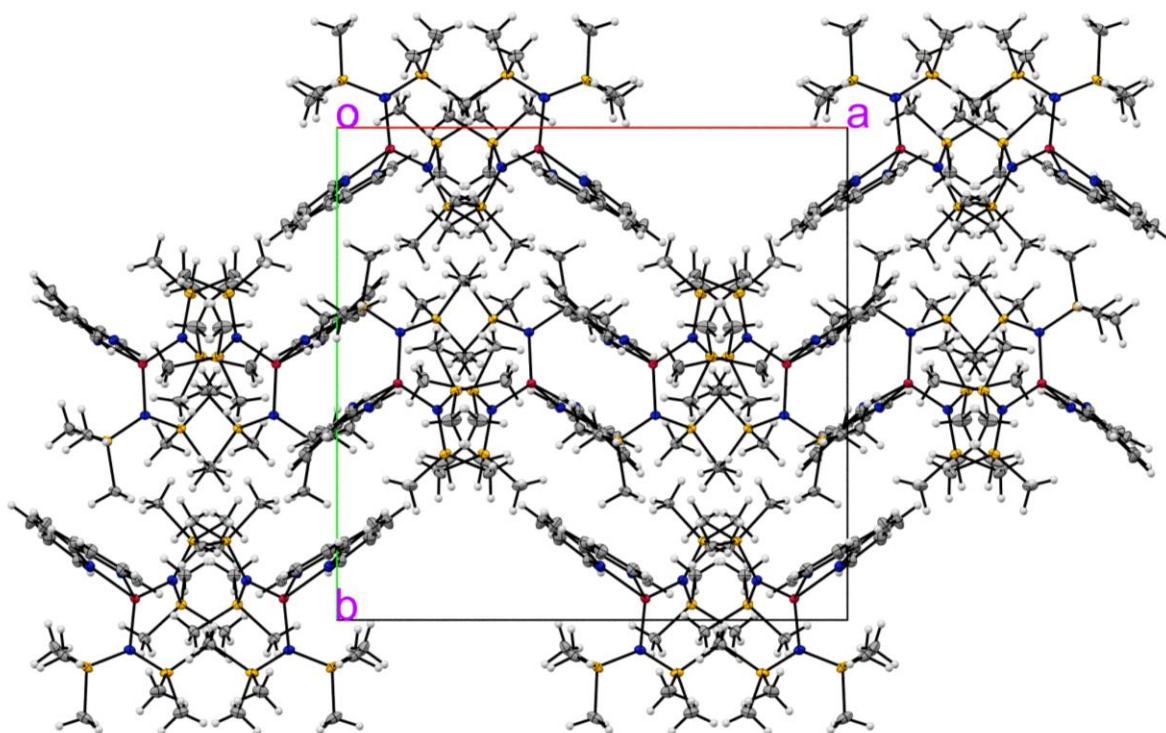




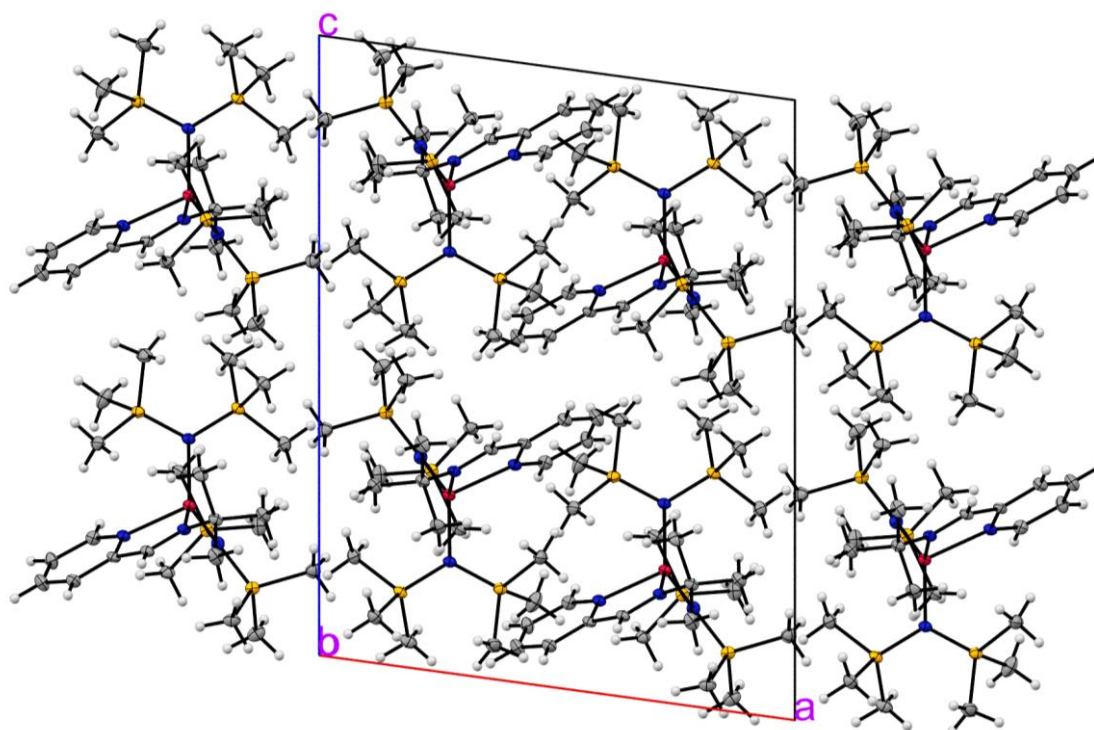
**Figure S 24:** Solid state packing illustration of  $[\text{Co}(\text{TMSA})_2(\text{DAD})]$  **3**, viewed down from the x-axis. The only notable short contacts (not shown here) observed when analyzing the packing situation were H–H contacts.



**Figure S 25:** Solid state packing image of  $[\text{Co}(\text{TMSA})_2(\text{DMAPY})]$  **4**, viewed down from the y-axis. Analysis of the short contacts and possible non-covalent interactions yielded only C–H and H–H interactions as described in the MS.  $\pi$ – $\pi$  interactions were not observed.



**Figure S 26:** Solid state packing diagram of  $[\text{Co}(\text{TMSA})_2(\text{BIPY})]$  **5**, viewed down the z-axis. While no direct  $\pi$ - $\pi$  interactions were observed, intermolecular  $\pi$ -H interactions as well as numerous C-H and H-H interactions were identified based on short contact analysis.



**Figure S 27:** Solid state packing diagram of  $[\text{Co}(\text{TMSA})_2(\text{IMPY})]$  **6**, viewed down the y-axis. Note the  $\pi$ -stacking interaction that can be seen from this extract. Short contact analysis revealed intermolecular  $\pi$ -H interactions as well as N-H and H-H interactions.

#### 4. References

- (1) Zemmann, J. Crystal structures, 2 nd edition. Vol. 1 by R. W. G. Wyckoff. *Acta Cryst* **1965**, 18, 139.